INTEGRATED FRACTURE AND STRESS CHARACTERIZATION, MISSISSIPPIAN "MERAMEC AND OSAGE" INTERVALS, STACK PLAY, CENTRAL OKLAHOMA

By
JOSHUA MICHAEL ANDREW BEDELL
Bachelor of Science in Geology
Oklahoma State University
Stillwater, Oklahoma
2017

Submitted to the Faculty of the
Graduate College of the
Oklahoma State University
in partial fulfillment of
the requirements for
the Degree of
MASTER OF SCIENCE
May, 2019

INTEGRATED FRACTURE AND STRESS CHARACTERIZATION, MISSISSIPPIAN "MERAMEC AND OSAGE" INTERVALS, STACK PLAY, CENTRAL OKLAHOMA

Thesis Approved:

Dr. Ahmed Ismail

Thesis Adviser

Dr. James Puckette

Dr. Michael Grammer

ACKNOWLEDGEMENTS

For my wife Callie. You have continued to hold our family together through this unexpected, difficult, but fulfilling journey we have been through. From high school sweet hearts to 5 years of marriage, 2 children, and half a dozen different homes, we have been through a lot. This document and the work therein, are a direct result of your determination, grit, and enduring love for me and our children Carolina and Channing. Thank you, I am truly blessed to have you in my corner.

I would like to thank my adviser, Dr. Ahmed Ismail. You are a true mentor who always wants what is best for your students and are willing to do anything necessary for us to succeed. You once told me that "if you ever had a son, you would want him to be like me." From a father to a father, there may be no greater compliment you could have given me. Although, I am not your son, I will always be your dear friend.

I would also like to thank Dr. James Puckette. I cannot write enough about you on this single page to give you the justice you deserve. You are maybe the kindest hearted, hardest working, and most disorganized person I've ever met. I was relieved to hear that you recently cleaned out your office – Congratulations! What an accomplishment! For better or worse, I suspect we will be seeing a lot of each other going forward. I can't wait to give you a hard time the next time we cross paths.

Next, I'd like to thank Dr. Michael Grammer. There is not one other faculty member who had a greater influence on me than you. You are a role model to me and you have inspired me to be a better geologist. I learned so much from our conversations and am fortunate enough to remember your most coveted words of wisdom. "Be precise" and "Carbonates are hard." Does that sound about right?

Lastly, thank you to the Geophysics Research Lab at Oklahoma State University which includes Rick Miller, Salman Abassi, and Md Zonaed Hossain Sazal for all of their help and their friendship as well. Oklahoma State and the Boone Pickens School of Geology have a special place in my heart and I truly feel honored and privileged to carry my degrees from this university.

Name: JOSHUA MICHAEL ANDREW BEDELL

Date of Degree: MAY, 2019

Title of Study: INTEGRATED FRACTURE AND STRESS CHARACTERIZATION, MISSISSIPPIAN "MERAMEC AND OSAGE" INTERVALS, STACK PLAY, CENTRAL OKLAHOMA

Major Field: GEOLOGY

Abstract:

Characterization of fractures, paleo-stresses, and the *in-situ* stress state is a major topic of interest among geoscientists and engineers in the petroleum industry. Fractures can significantly influence reservoir quality, while both fractures and the stress-fields impact all phases of hydrocarbon exploration and development. Years of study have resulted in dozens of different techniques to detect and characterize fractures and stresses, and their ensuing impact on reservoir quality. However, integrated fracture characterization studies are rarely implemented into exploration projects due to lack of essential datasets, budgets, and time constraints, which in many cases, negatively impact subsequent exploration and development strategies. Previous studies over the STACK play in central Oklahoma have indicated that naturally fractured zones may have a potential impact on production within the "Meramec and Osage" intervals. Therefore, this study aimed to characterize fracture density and orientation, and stress-regimes within the "Meramec and Osage" intervals in the STACK play through an integrated approach. This approach is based on the analysis of 3D seismic data, petrophysical data from six wells, two cores and one Formation Micro-Imaging (FMI) log. Density and orientation of seismic-scale fractures were estimated based on a generated suite of seismic attributes and a discrete fracture network. Density of log-scale fractures was inferred from the analysis of the petrophysical, cores, and FMI log data, while orientations of these fractures were determined only from the FMI log. Both modern and ancient stress regimes were estimated from the analyses of the seismic and the FMI log data. Orientations of the natural fractures and drilling induced fractures were used to estimate the *in-situ* and paleo-stress-fields. Although the scale of fractures detected by each of the four datasets was different, density and orientations of the different-scale interpreted fractures were consistent. Additionally, fractures were shown to have an overall negative impact on the "Meramec's" reservoir quality but had a positive influence on reservoir quality in the "Osage" interval. The results of this study showed that the integrated approach of fracture characterization utilizing multi-scale datasets can better improve our understanding of fractures and the early and contemporary stress states of the reservoir, thereby reducing risk associated with petroleum exploration, drilling, and completion activities.

TABLE OF CONTENTS

LIST OF EQUATIONS

LIST OF FIGURES

Figure Page

CHAPTER I

INTRODUCTION

1.1. Motivation and Objectives

The "STACK" (Sooner Trend Anadarko Canadian Kingfisher) play is located within the Anadarko Basin in Central Oklahoma. It is a relatively new unconventional play brought to life in older oil fields due to advancements in horizontal drilling and completion techniques. Although the STACK is rich in legacy well data, surprisingly, the nature of the fractures and the stress regimes, and their potential impact on the quality of the STACK reservoirs, especially within the Mississippian "Meramec and Osage" intervals, are poorly understood. The Mississippian "Meramec and Osage" intervals, sometimes referred to as the "Mississippian Limestone," are often described as tight mixed siliciclastics and carbonates and were rarely historical conventional targets. Although relationships from multi-scale (e.g., seismic, log, core, etc.) fracture characterization studies have been recognized around the world (e.g., Shafiei et al., 2018; Hesthammer and Fossen, 2003; Liu et al., 2015) to the best of my knowledge, there is no such study for the STACK reservoirs. Fractures and the *in-situ* and paleo stress regimes can be key drivers to reservoir quality and well performance.

The lack of fracture and stress regime studies over the STACK in the past is most likely due to the shortage of advanced datasets required to complete such studies. This study benefits from recent modern seismic, core descriptions, petrophysical analyses, and image logs made available by Devon Energy. The study aims to utilize an integrated approach to characterize

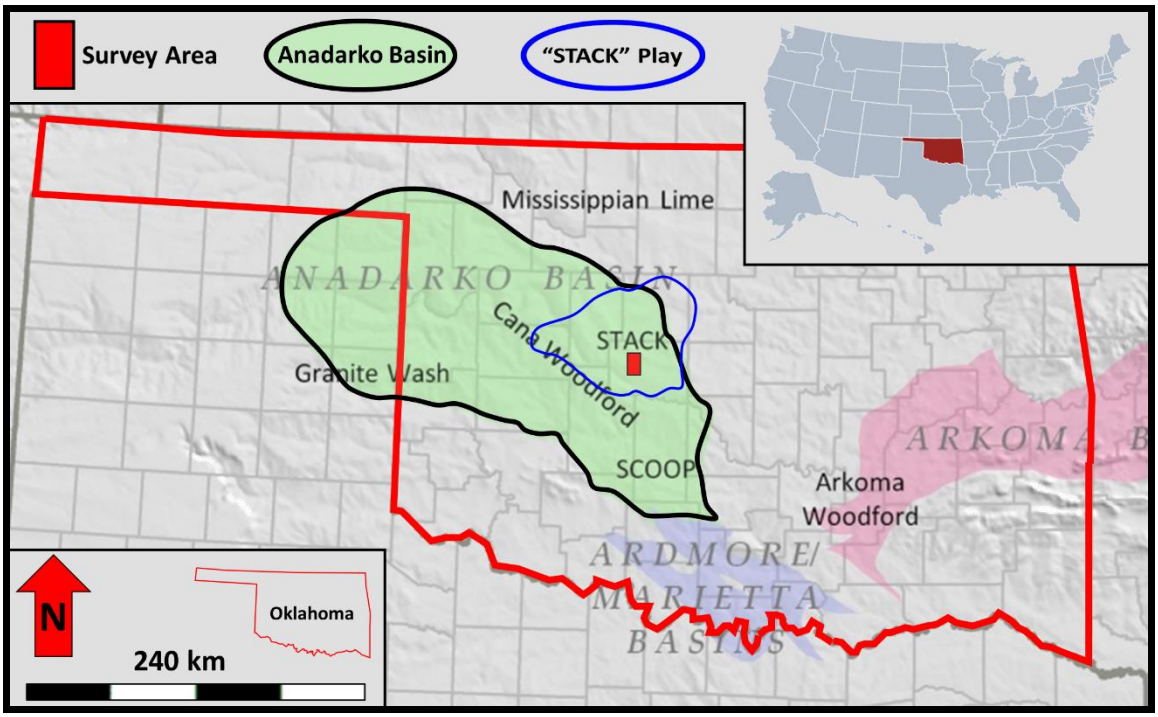

Figure 1: A map showing the location of the study area within the "STACK" play of Central Oklahoma. Modified from IPPA, 2018.

1.2. Definitions and Fracture Origins

The occurrence of fractures is most often associated with brittle deformation in the upper crust that forms where stress builds up to levels that exceed the local rupture strength of the crust. This results in a breakage of crystal lattices at the atomic scale that can then be extrapolated to large scale discontinuities such as faults (Fossen, 2010). The investigated fractures in this study refers to the discontinuities that occur in rocks due to brittle/semi-brittle deformation (Ameen, 2003). These types of fractures can be either natural or induced fractures. Natural fractures are caused by natural deformation of the rock and can include: faults, cracks, joints, veins, and stylolites. Induced fractures are formed artificially by core handling, coring, drilling, fluid injection, etc. (Ameen, 2003).

The in-situ stresses are the present-day natural stresses acting on the earth's crust. They are the result of different mechanisms including: 1) gravitational stresses due to the weight of the overburden, 2) Current tectonic stresses related to present day tectonic forces or 3) remnant/residual stresses locked in the rock during past episodes of tectonic and gravitational stresses (Ameen, 2003). Paleo-stresses are the ancient stress states that were controlled by the same criteria as the in-situ stresses but can only be in interpreted using identifiable geologic features that give an indication of remnant stress regimes.

The term fracture characterization in this study is used to encompass the detection, diagnosis, quantification, and qualification of fractures (e.g., orientations, densities, length, etc.). Stress characterization, however, determines the orientation and estimates the relative and/or absolute magnitudes of the three principle in-situ and paleo-stresses (maximum horizontal stress, minimum horizontal stress, and vertical stress, referred to as σ_H, σ_h, and σ_v, respectively) (Ameen, 2003). In this study two general scales are used when referring to the size/scale of fractures, which are seismic-scale and log-scale. Seismic scale here is defined as any feature that can be detected by the naked eye or in some cases, below the naked eye when calculated from seismic attributes. The seismic-scale for this study is thought to encompass all features above ~3 meters (12 feet) vertically (theoretically detectable vertical limit). Log-scale in this study lumps in the resolution from core interpretations and ranges from mm's to a couple meters into the formation.

1.3. Fracture and Stress Characterization Approaches

Fractures and stress can often be described using different data including seismic, log, core, and thin sections. Seismic techniques for fracture characterization include: attribute generation, discrete fracture networks, shear wave splitting, and seismic inversion (e.g., Tinker et al., 2004; Pranter et al., 2004; Chopra and Marfurt, 2007; Lei et al., 2017). The vertical and lateral

resolution of the seismic data is often below the acceptable level for interpretation and the results often must be verified with hard data (Hesthammer et al., 2001). Basic well logs, such as the caliper log and density log by themselves, are useful in detecting the presence of fractures but have severe limitations as they can't determine fracture orientation or size (Shalaby and Islam, 2017; Suau and Gartner, 1980). Dipmeter and image logs are extremely useful in determining small scale fracture density and orientation but only measure the surface of the borehole leaving many unknowns about the presence of fractures in the remaining reservoir. Core descriptions of fractures are beneficial in describing very small-scale fractures, but the results can be misleading since the core is a 1-dimensional dataset within a complex 3-dimensional body (Hesthammer et al., 2001; Wang et al., 2019).

Although all these techniques are capable of detecting fractures, each technique has limitations in evaluating the size, distribution, and orientation of fractures. Therefore, in-order-to obtain a more robust fracture characterization, the integration of multiple techniques is a necessity for better characterization of fractures. This study has taken an integrated approach by compiling previous works, utilizing advanced seismic analyses from a modern seismic dataset, innovative petrophysical studies, and core descriptions to characterize fractures, in-situ, and paleo-stresses in the "Meramec and Osage" intervals of the STACK play. The outcomes of this study will improve our understanding of the fractures and the in-situ and paleo-stresses of the "Meramec and Osage" intervals of the STACK play, which further reduces the risks associated with petroleum exploration, drilling, and completion activities.

CHAPTER II

GEOLOGIC BACKGROUND

The term "Meramec and Osage" (Fig. 2), sometimes referred to as the "Mississippian Limestone," is used in this study to avoid the unsettled nomenclature and age determinations of the "Osage and Meramec" sections in Central Oklahoma.

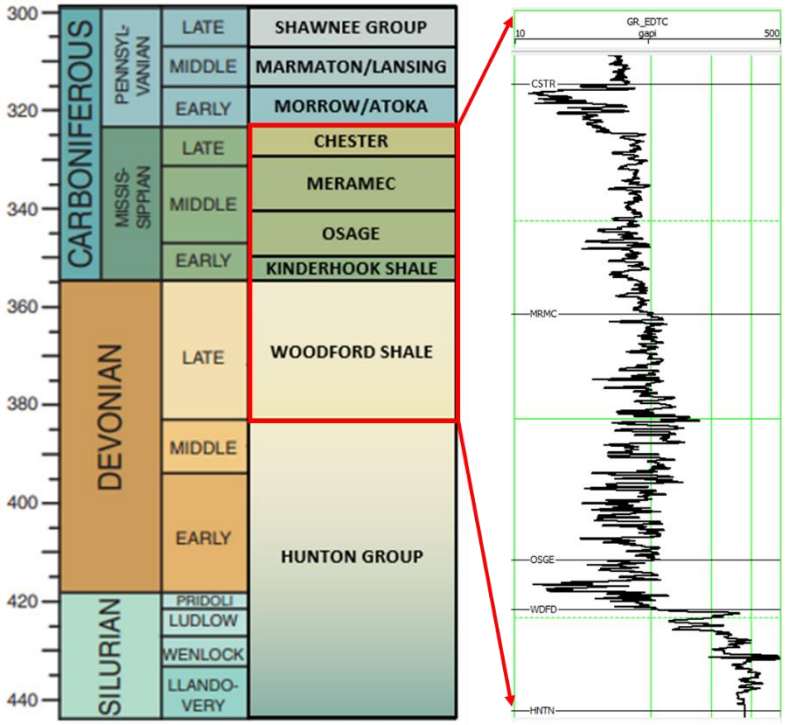

Figure 2: Left: Stratigraphic column in the STACK play of the Anadarko Basin. The Mississippian "Meramec and Osage" intervals are highlighted in red. Right: Gamma Ray log from the Chester through the Woodford Shale shows the typical log signature of the "Meramec and Osage" intervals and how it generally becomes less calcareous from the "Osage" into the "Meramec" (modified from Walker et al., 2018).

The Mississippian “Meramec and Osage” intervals are encompassed within the Anadarko Basin of Oklahoma and Texas in the mid-continent of North America (Fig.3). The Anadarko Basin is bounded by the Amarillo-Wichita uplift on its southern flank and the Nemaha uplift to the east. It is classified as a foreland basin that is asymmetric in shape with a sedimentary column that exceeds 12,000 meters (~40,000 feet) (Perry, 1989). From Cambrian to Mississippian time, the area of the Anadarko Basin was located near the equator and was predominantly covered by warm, shallow seas with carbonate deposition being the dominant form of sedimentation (Price and Grammer, 2018). The “Osage” section, which is more carbonate rich, was likely deposited in these conditions. A gradual transition to more siliceous sedimentation began to occur throughout the mid to late Mississippian where more argillaceous sections are observed such as the “Meramec” interval (Childress and Grammer, 2018; Price and Grammer, 2018). The Late Mississippian was subject to a reintroduction of tectonism as significant plate collisions resulted in the Ouachita orogeny and formation of the Ancestral Rocky Mountains, which had major influences on the present-day basin configuration. (Higley et al., 2014).

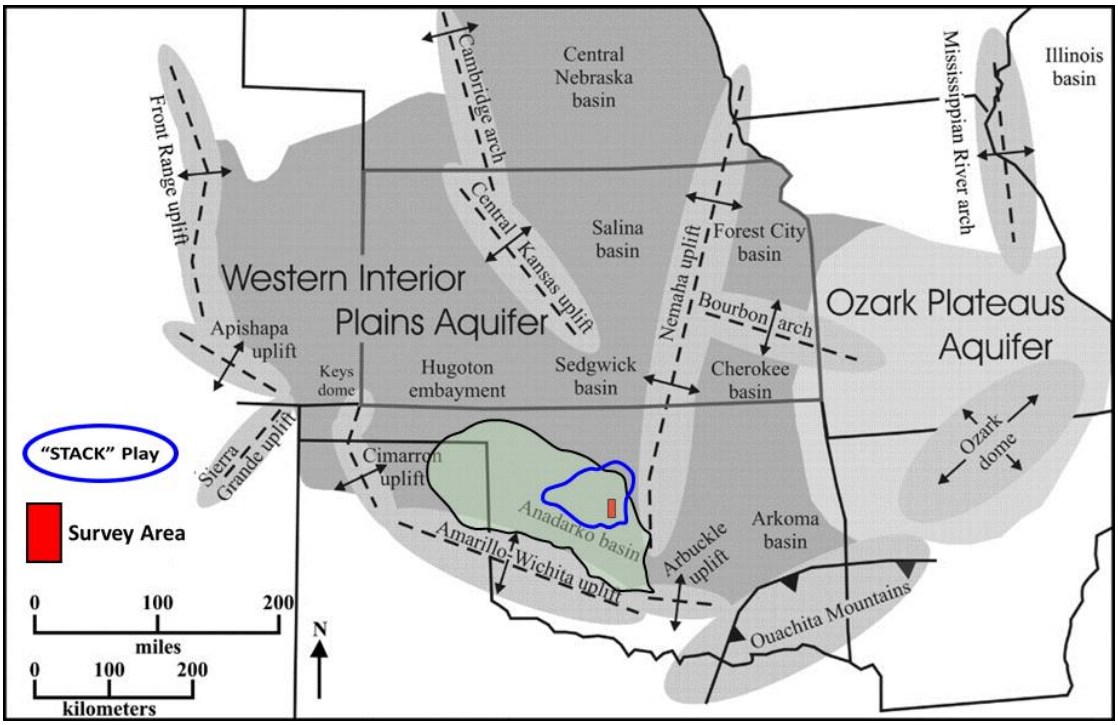

Figure 3: Schematic of the Anadarko Basin and surrounding structural features. Anadarko Basin in green. STACK play outline in blue. Survey area outlined in red filled box (modified from Carr et al. 2005)

2.1. Tectonic Framework

Perry (1989) divided the Anadarko Basin's structural history into four periods: (1) Precambrian crustal consolidation, (2) late Precambrian to Middle Cambrian aulacogen development, (3) Cambrian through Early Mississippian development of the southern Oklahoma trough and (4) Late Paleozoic tectonism associated with development of the Anadarko basin on the northwestern flank of the trough.

During the Early- to Middle- Cambrian, rifting and deep-seated faulting associated with the Ouachita fold belt began to form the southern Oklahoma Aulacogen. Although, there is little direct evidence, it is likely that many of the faults formed during the initial rifting phase were reactivated during the subsidence period (Ham et al., 1964; Wichham, 1978). During the post rifting phase, throughout the Middle Cambrian to Late Mississippian, the area was mainly

influenced by thermal cooling, subsequently creating the Anadarko Basin (Wittman, 2013). During the late Paleozoic (Late Mississippian into Permian) a major episode faulting occurred in much of south-central Oklahoma. Published literature suggests the prevalence of left-lateral faulting, such as the large Washita Valley fault system 80-100 km (~50-60 miles) to the south of this study was most common (Moody and Hill, 1956; Tanner, 1967; Thorman, 1969; Wickham, 1978; Butler, 1980; McLean and Stearns, 1983; Harding, 1985; Budnik, 1986; Cox and VanArsdale, 1988). The specific chronology and mechanisms for the tectonic activities though is unclear and is subject to strong disagreement (Denison, 1982; Cox and VanArsdale, 1988). Early surveys postulate northeast transported thrusting and later left-lateral movement throughout the Pennsylvanian for the province (Brewer et al., 1983). Regardless, the dominant geochronological structural influence appears to be that of left-lateral movement and generally east-west compression during the Mississippian and Pennsylvanian periods.

2.2. Stratigraphy and Sedimentation

The "Meramec and Osage" intervals in the study area, have not been described in detail in the literature. Alternatively, the "Mississippian Limestone" in Northern Oklahoma, acts as the time equivalent analog that has been thoroughly described. It has been chronostratigraphically correlated from outcrops in Northern Oklahoma, Southern Kansas, North-West Arkansas, and South-West Missouri all the way to the subsurface in Kingfisher County Oklahoma (Stukey et al., 2018). During much of the Mississippian, relatively shallow subtropical epeiric seas persisted and a mixed carbonate-siliciclastic environment was established over the area (Price and Grammer, 2018) (Fig. 4). The "Meramec and Osage" intervals in the study area have been generally described as siliceous limestones and calcareous siltstones (Cullen, 2017) that are believed to

have been deposited on a regionally pervasive, distally steepened carbonate ramp prograding from NW to SE (Childress and Grammer, 2018; Price and Grammer, 2018).

Price et al. (2018) described the Osagean strata as a series of limestones, siltstones, and shales. The "Meramec" interval in the study area was described as a calcareous siltstone and is approximately 50% silt < 60 µm in diameter with significant calcite cement with mica and pyrite accessory minerals (Cullen, 2017). The depositional environment of the "Meramec" interval in the study area is still debated but has been described as a subaqueous delta complex that is defined by the presence of low angle (< 1°), shore parallel clinoforms that were fed by fine grain riverine input systems and deposited primarily by longshore basinal currents within or below the storm wave base (Price et al., 2017; Patruno et al. 2015). These clinoforms have been interpreted to exhibit a progradational pattern to the southeast and exhibit similar facies trends across each clinoform due to the depositional environment (Price et al. 2017).

Generally, there is a good correlation between fracture occurrence and the calcite content within the "Meramec" and "Osage" intervals (Wang et al., 2019). Most often, an increase in calcareous cement or sediment will result in an increase in fracturing (Wang et al., 2019). This potentially could add to the total porosity and permeability if the fractures were open and formed a connected network. Wang et al (2019) and Cullen (2017) noted that the vast majority of the fractures in the "Meramec and Osage" intervals appear to be completely mineralized but could still be acting as planes of weakness that can help facilitate the propagation of induced fractures.

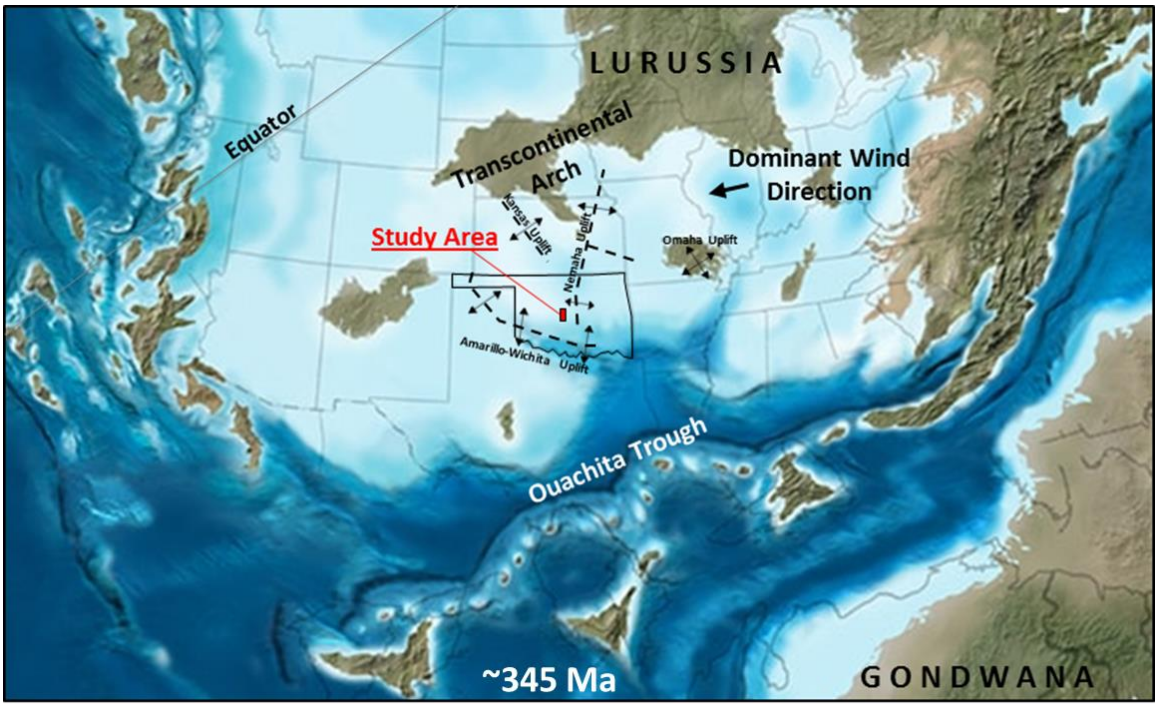

Figure 4: Paleogeographic map during the Mississippian (~345 Ma) illustrating that much the mid-continent was covered by shallow seas along with simultaneously occurring nearby tectonic events promoting the deposition of mixed siliciclastic carbonate material as we see in the "Meramec and Osage" intervals. (map and interpretation modified from Blakey, 2013; Carr et al., 2005, Wang et al.,

CHAPTER III

DATA AND METHODOLOGY

3.1. Data

This study has utilized multiple data sets to characterize fractures and in-situ and paleo-stresses through an integrated approach. These data sets include a 3D seismic survey over 324 square kilometers, 10 wells with modern log suites, and two STACK cores (Fig. 5), all of which were donated by Devon Energy Corporation. Data analyses and interpretations were completed using multiple industry software packages. IHS's Kingdom was used for basic seismic and log evaluation. CGG's Hamson-Russell software packages including Geoview, was used to for seismic well-ties and horizons picking. CGG's InsightEarth was used for advanced seismic fracture characterization. Rick Allmendinger's Stereonet 10 software was used to plot and visualize fracture strike and dip. Industry collaboration with Devon Energy Corporation, Cimarex Energy, Nutech Energy, and CGG took place as needed. A modified version of the Hesthammer and Fossen (2003) integrated core to seismic fracture characterization workflow was adopted for the completion of this study.

3.1.1. Seismic Data

The seismic data used in this study is a 3D seismic volume acquired in 2012 by Dawson Geophysical, and processed by CGGVeritas. It has a sample rate of 2 milliseconds, a trace length of 6 seconds, and a bin spacing of 25 m (82.5 feet). The area of coverage for the data set used is approximately 324 square kilometers (125 square miles) consisting of 1428 seismic inlines and

and 564 seismic crosslines (Fig. 5). The seismic data was migrated using the advanced orthorhombic pre-stack time migration (PSTM) to account for both the VTI and HTI anisotropy. The seismic data shows good quality throughout the survey area.

Seismic vertical resolution is the minimum vertical thickness of a layer required to produce a seismic reflection that is visible in seismic and depends on the seismic frequency or wavelength. A peak dominant frequency 35-40 Hz was determined along with a bandwidth of 15 Hz - 65 Hz for of the available seismic data. Accordingly, the vertical seismic resolution was determined using equation (1), (Redger, 2015), and was found to be approximately 18-23 m (60-75 feet) at target depth which is well within this study's range of investigation. The "Meramec and Osage" intervals exceed 150 m (~500 feet) in thickness at target depth (over 3000 m deep) consistently throughout the study area.

$$\left(\frac{\lambda}{4}\right) = \frac{v}{4f}$$

Where: λ = wavelength, v = velocity, and f = frequency. (Eq. 1)

3.1.2. Well Log Data

Ten wells drilled at various depths along with differing modern log suites were available for this study (Fig. 5). Of those ten wells, only six were given detailed fracture petrophysical evaluations due to some of the wells either lacking the appropriate log suites or not having logs that encompass the full "Meramec and Osage" intervals. The logs required for the fracture petrophysical evaluation included: sonic logs, density logs, caliper logs, resistivity logs, gamma ray logs, and porosity logs. Furthermore, all ten wells coalesced in the northern half of the survey, so this project focuses its efforts there.

3.1.3. Formation MicroImaging (FMI) Log Data

An FMI log was provided by Devon Energy Corporation that proved to be useful (Fig. 5). The log was run on water-based mud which significantly improves the data quality, resolution, and subsequent interpretability of the image log. The FMI log is located near the northwest corner of the seismic survey. This is an imperative dataset as it is the only other dataset aside from the seismic volume that provide fracture orientation information and can link the seismically characterized fractures to the core/log characterized fractures.

3.1.4. Core Data

Two non-oriented core were available for this study within the survey area (Fig. 5). Well D was cored ~230 meters (750 feet), into the "Meramec and Osage" intervals along with the lowermost Chester interval and uppermost Woodford section. Well B contained the second core which covered a 55 meter section (180 foot), with the uppermost ~6 meters (20 feet) from the lower "Osage" interval with the rest being Woodford. Only the "Meramec and Osage" interval interpretations are included in this study. The primary purpose of the core study was to (1) provide "hard data" "ground truthing" for the occurrence of fractures detected in seismic and FMI log and (2) to provide another relative fracture density dataset that could be compared to the FMI log and petrophysical evaluations.

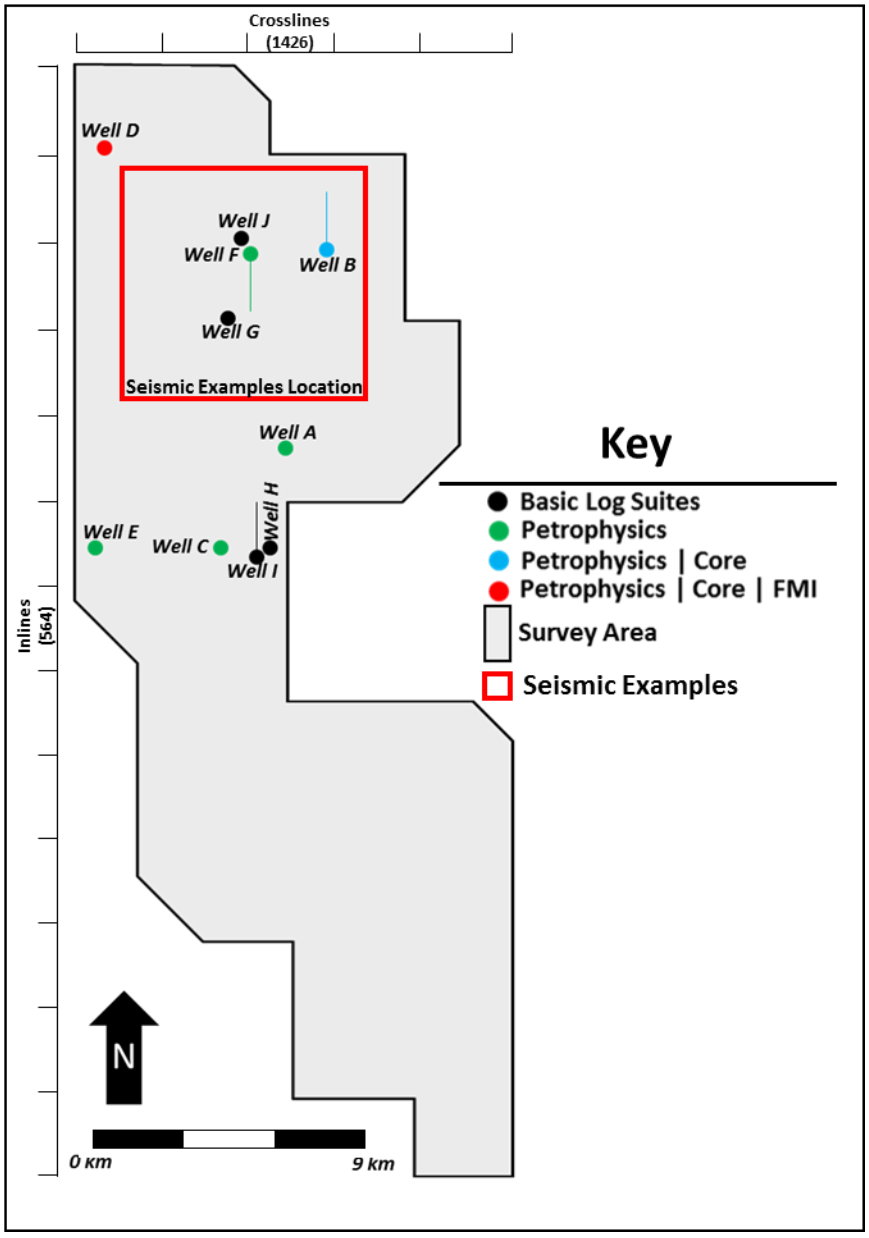

Figure 5: Outline of the 3D seismic survey area with the 10 well's relative locations to the survey area shown. Black circles indicate wells with basic log suites, green circles indicate wells with petrophysical analysis, blue circles indicate wells with petrophysics and core, and red circles indicates wells with petrophysics, core, and FMI logs. The wells sticks indicate horizontal wells and their orientation.

3.2. Methodology

The workflow for this study started with a comprehensive literature review to better understand the tectonic and structural framework and depositional system of the "Meramec and

Osage" intervals and to determine the potential controls on fracture architecture. An integrated approach was followed to characterize large-to-small scale fractures and stress relationships using the subsequent seismic, log, and core datasets (Fig. 6).

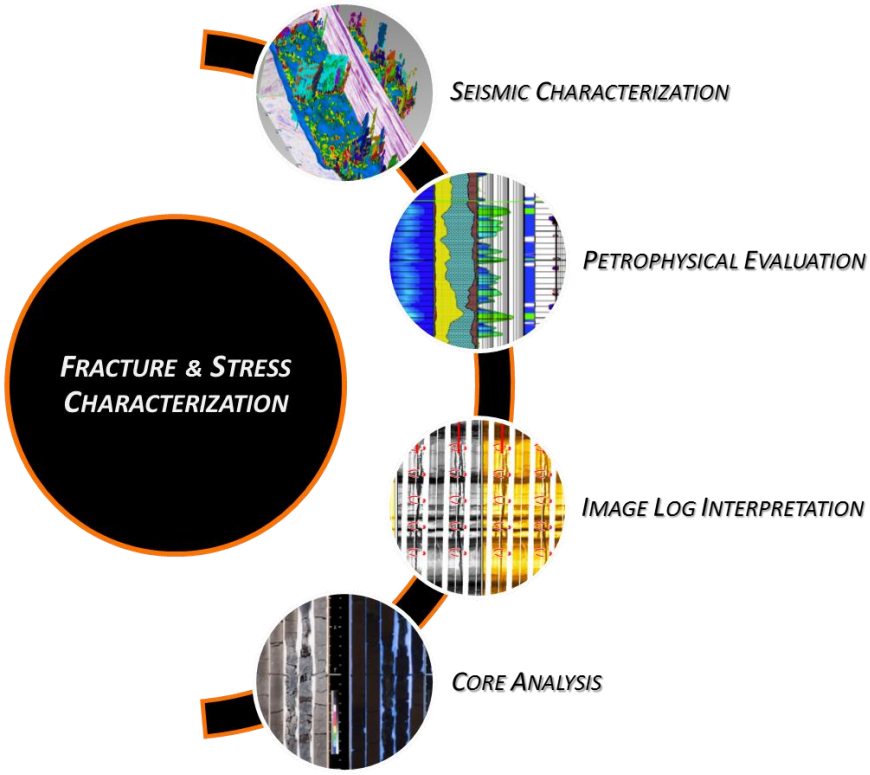

Figure 6: Schematic illustrating the overall general large-to-small workflow including seismic characterization, petrophysical evaluation, image log interpretation, and core analysis. The results of each analysis complimented each other resulting in a superior integrated fracture and stress characterization.

3.3. Seismic Fracture Characterization Workflow

The seismic volume was analyzed using IHS's Kingdom software for basic data evaluation. CGG's Hampson-Russell Geoview software was used for tying the wells to the seismic data, horizon picking, and for other basic seismic and well log interpretation. The CGG's InsightEarth FaultFractureSpark software package was utilized to condition and manipulate the seismic volume for advanced fracture interpretation including: attribute generation, building of

the Discrete Fracture Network (DFN), fracture vector glyphs generation, and generation of interactive rose plot diagrams. Figure 7 illustrates the general seismic characterization of fractures and stress workflow carried out in this study.

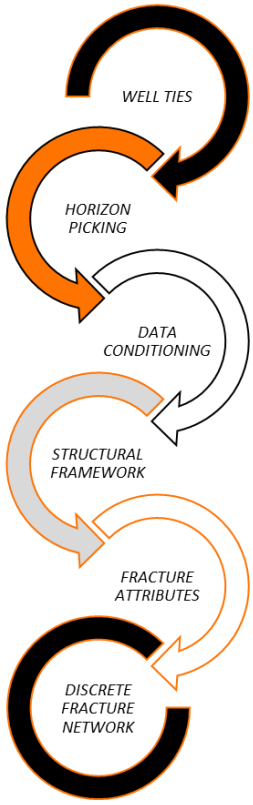

Figure 7: Schematic illustrating the overall general steps of the seismic characterization workflow.

3.3.1. Well Ties and Synthetic Wavelet Extraction

Often the first and most critical step of analyzing seismic data is registering the well data to the seismic data, or "well tying," to obtain time to depth relationships. This procedure is the foundation for all other subsequent work as it creates connections between actual geological information (i.e., formation tops, log signatures, etc.), which is in depth, and the individual reflection events in the seismic data, which is in time. This is also key to attaining a visual understanding of the seismic resolution as it relates to the target intervals as defined in the

interpreted well logs. Finally, the tied wells act as a quality assurance measure when interpreting seismic horizons as they essentially are control points and "ground truth" interpretations. The well tie process was accomplished utilized CGG's Hampson-Russell Geoview software package.

The first step in the well-to-seismic correlation process is to generate a synthetic seismic wavelet, or seismogram. In this study, this was accomplished utilizing the product of the velocity values from the sonic log and the density values from the bulk density log to create an acoustic impedance log that was subsequently converted to a synthetic seismic reflectivity series. Calculating the synthetic was completed based on the convolution model which involves convolving the reflectivity value with a band limited wavelet and adding random noise (Leckie et al., 2000). This extracted wavelet functions as a link to the seismic data (traces) and the geology (reflection coefficients).

Once this was completed, the next step was to actually match reflective events by correlating the synthetic traces generated from the well logs to the actual seismic traces. Interpreters will typically identify strong seismic reflectors, or a distinct sequence of reflectors, that can be used as a starting point in correlating the two datasets. In this case, the Woodford interval, which is generally composed of a 30-60 m (~100-200 feet) of highly organic rich shale, creates a bright distinct reflector which can usually be differentiated from other horizons and is used as the first tie point. From here, the synthetic wavelet can be "stretched" or "squeezed" to obtain the highest correlation coefficient. Generally, the highest quality well ties are those that contain the least amount of "stretching" and "squeezing" while obtaining the highest correlation coefficient. Well ties in this study appear to be of a good quality demonstrating >75% correlation coefficients between synthetic and true seismic records. This is mainly because both seismic and well log data are generally of good quality. An example of the well tie from Well B is shown in Figure 8.

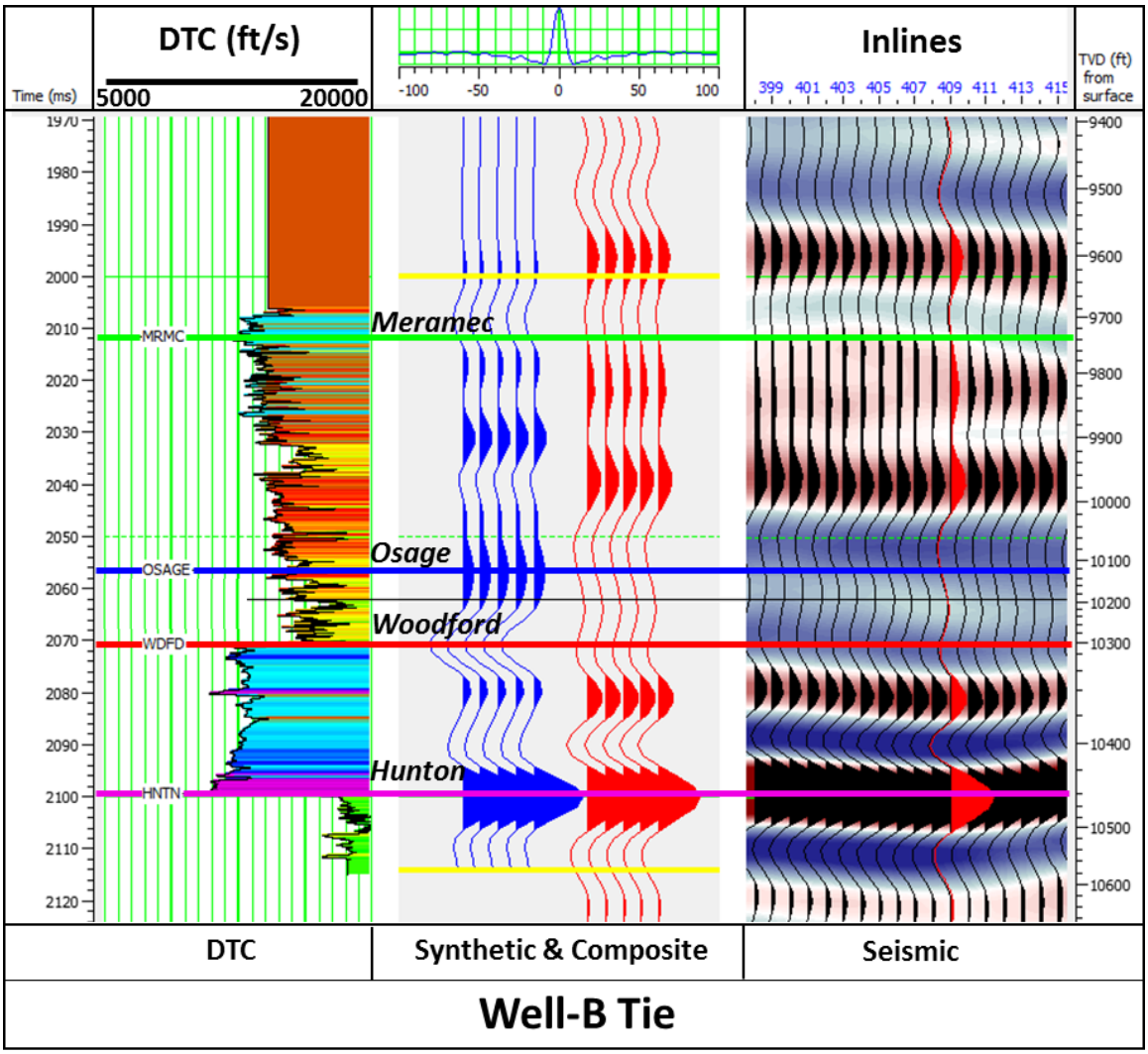

Figure 8: Correlation of well log data to seismic data (well tie) of the Well B from the synthetic seismogram generation. A correlation coefficient value between the synthetic and seismic data, the blue and red traces, respectively, was determined to be approximately .76. The corrected sonic log is shown in the first track with well tops of interest labeled for reference.

3.3.2. Horizon Picking

After establishing high quality well ties, the interpreted "Meramec", "Osage", and Woodford horizons were picked in Geoview software. The horizon picking started at the well ties and worked to the edges of the seismic survey. Every 5th inline and crossline was manually picked, thus creating a grid to act as control points for the subsequent autotracking. Difficult, or

more structurally complex, areas were interpreted manually along every single applicable inline and crossline to ensure computer generated picking algorithms did not create invalid seed points. An example of the picked horizons is shown in Figure 9 below.

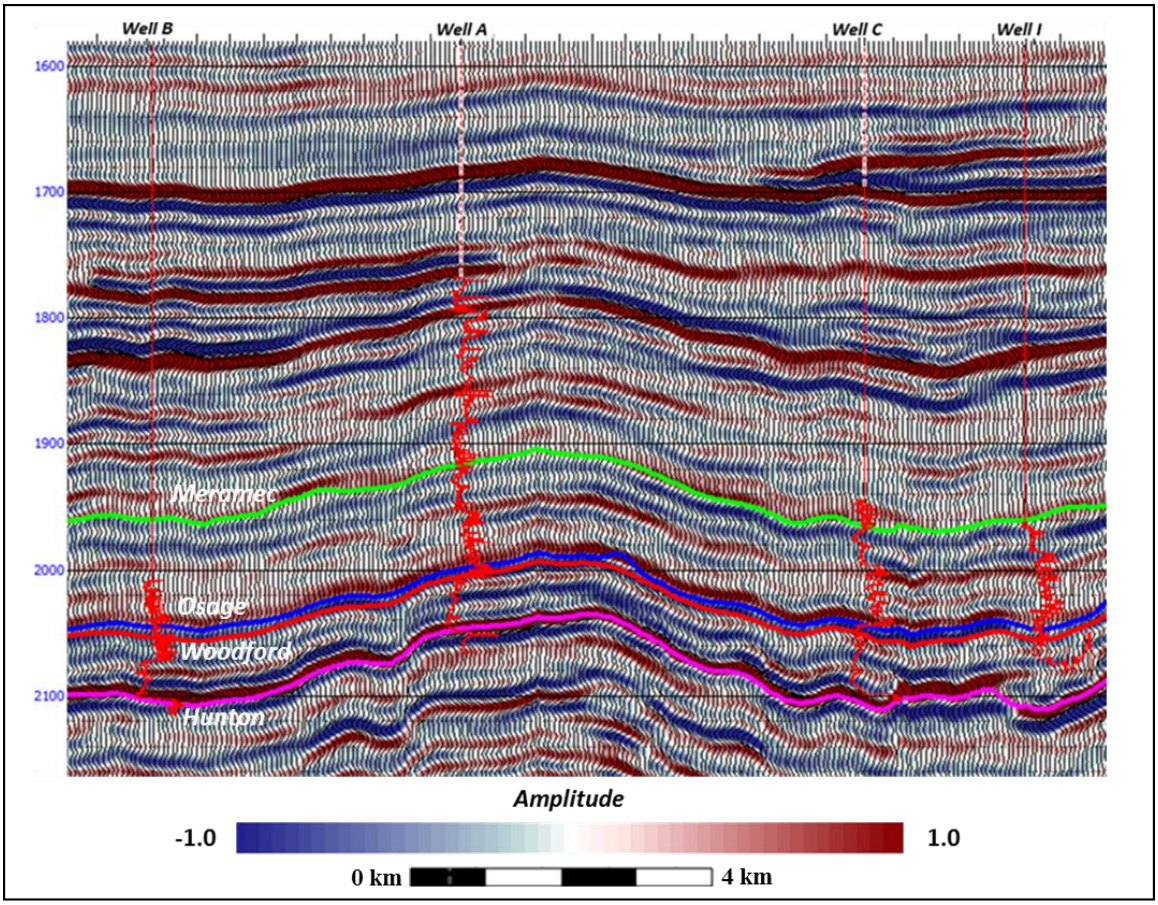

Figure 9: Example of horizons picked on an arbitrary line between all wells that penetrate through the Woodford interval. The synthetic log curves are overlain on the seismic section to illustrate velocity changes within the displayed section. The "Meramec," "Osage," Woodford, and Hunton horizons are displayed by the green, blue, red, and purple lines, respectively.

3.3.3 Seismic Data Conditioning and Manipulation

Although the seismic dataset was of very good quality, several conditioning and manipulation steps were applied in InsightEarth to reduce noise, amplify fracture signal, speed up processing times, and to focus on the intervals of interest. Generally, with high quality seismic data sets, the minimal amount, or least invasive data conditioning and noise filtering the better.

Intensive data cleaning can result in the deletion of real reflectivity data, which would otherwise ultimately become real geological information. With this in mind, four data conditioning and noise reduction procedures were applied to this dataset. These procedures are iterative and build off each other in order to improve the quality of the subsequent conditioning step.

First, the non-conditioned seismic amplitude volume (Fig. 10a) was used to generate a Horizon Orientation attribute (Fig. 10b) in InsightEarth Software. This attribute contains strike and dip vector information of the seismic reflectors and is used in subsequent conditioning and attribute generation steps. The second step was to apply a footprint removal filter (Fig. 10d), which is a coherent noise filter that removes acquisition footprint artifacts (i.e., striping) uses the original seismic volume and the Horizon Orientation attribute as inputs to remove the majority of any acquisition footprints. The Horizon Orientation attribute significantly increases the quality of the footprint removal as it allows the footprint removal to be dip oriented, so that it does not attenuate steeply dipping features in the data. Fortunately, this survey only had visually noticeable footprints in the upper 200 ms of the volume along both the inlines and crosslines. Being that the zones of interest lie between 1700 ms and 2400 ms there was likely very minimal footprint interference at those time depths so only one footprint removal was applied to the shallow depths. This was done by using a tool in InsightEarth to measure the distance between acquisition footprints to ensure only acquisition footprint noise is removed.

Finally, a statistical filter, which removes random noise, was applied to the conditioned seismic volume to resolve genuine seismic reflectivity data (Fig. 10e). The statistical filter uses the Horizon Orientation volume to help preserve steeply dipping features and properly orient the filter operator so that it stays perpendicular to events (CGG- Geosoftware, 2015 and 2018).

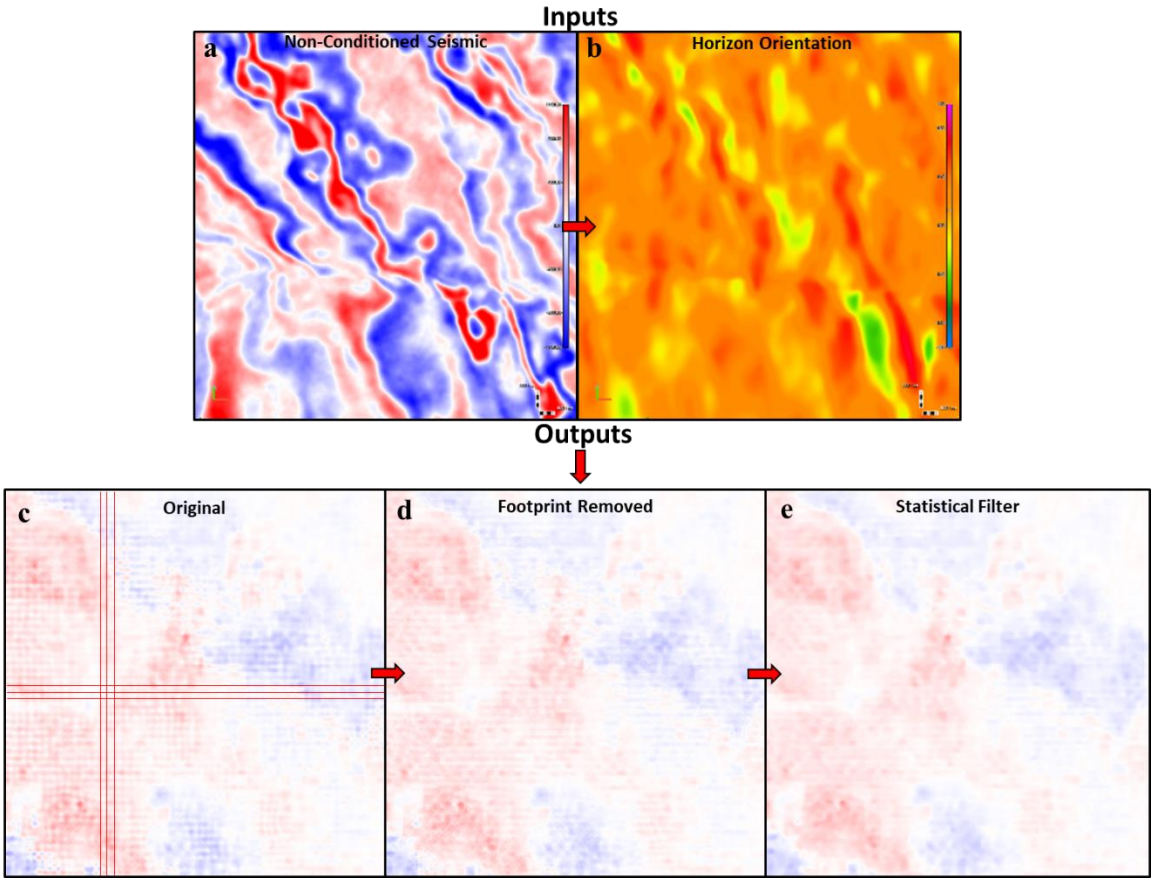

Figure 10: Seismic examples at 200ms from the location of the inputs (i.e., non-conditioned seismic and Horizon Orientation) and outputs (i.e., Footprint Removed and Statistical Filtered volumes). An example of the original volume is also shown to illustrate the improvement.

3.3.4. Large Scale Structural Framework

Before a more detailed higher resolution small-scale fracture characterization takes place, it is important to effectively image all of the larger fractures/faults visible to the naked eye in the seismic volume. This is important for three main reasons: (1) small scale fractures cannot be properly interpreted without the context of the associated larger faults. (2) Large scale faults often give an indication of the in-situ and paleo-stress states. (3) Large-scale faults are often intrinsically related to smaller scale faults/fractures (Butler et al., 1976; Fosse, 2010). This step was completed in InsightEarth's FaultSpark interpretation package using the previously

conditioned seismic volume. A series of coherency class attributes, tuned for larger scale faults, were used in an iterative built-upon-each other fashion in order to obtain accurate strike and dip information from the faults.

Using the generated seismic attributes as inputs, most of the faults/fractures visible to the naked eye were extracted as editable point sets. The next step was to manually edit the fault pointsets by deleting erroneous portions and/or projecting them further where faults were not fully imaged. Once quality controlled, the fault pointsets were converted to surfaces that were used for later interpretations (Fig. 11).

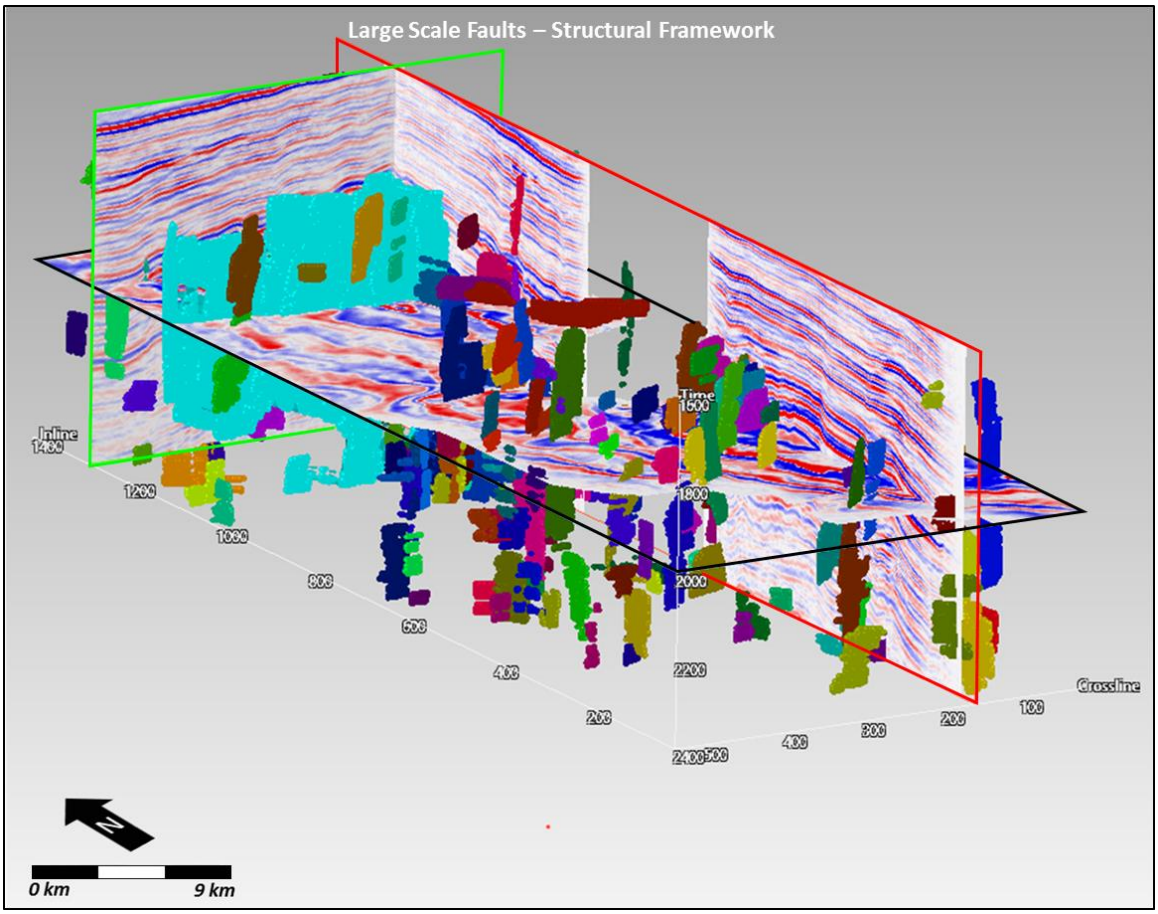

Figure 11: Figure shows extracted large scale fault surfaces over the seismic volume. This volume was used to establish the larger scale structural framework.

3.3.5. Geometric Attributes for Fractures Detection

After the larger scale structural framework was established, a robust fracture analysis was carried out in InsightEarth's FractureSpark interpretation package. The first step was to generate a series of coherency and curvature class attributes that again were used in an iterative built-upon-each other fashion to continually improve the subsequent attribute. There are numerous options for attribute generation, and various settings for each, but for the continuing purpose of characterizing fractures, geometric attributes, such as coherency and curvature class attributes were used in this study. These attributes are the most reliable and accurate at highlighting structural features (Chopra and Marfurt, 2007; Marfurt et al., 1998).

The Horizon Orientation attribute volume and the conditioned seismic volume were used again as inputs to generate a Horizon Edge Stack volume, which is a coherency class attribute. The parameters for this attribute were specifically designed for fracture detection/imaging as the "3D Diameter" operator, which controls the trace count, was set to be very short (i.e., 3 traces) to increase the density of measurements to include smaller fractures. Additionally, the "Horizon attenuation" setting was set to 95% to attenuate the horizon leakage associated with fractures, resulting in better fracture imaging (Fig. 12). The next coherency attribute created was the Fracture Highlight attribute, which helps visualize fracture probability, occurrence, and density. This procedure uses the Horizon Edge Stack volume attribute, as an input to generate Fracture Highlight attribute (Fig. 12). The settings for this step are tuned to minimize noise and maximize fracture signatures, especially those of which are below the resolution of the naked eye.

Using the Horizon Orientation attribute described in section 3.3.3 and the conditioned seismic volume as inputs, six curvature attributes, tuned specifically for fractures, were also computed over the conditioned 3D seismic volume. The generated curvature attributes include: K1, K2, Mean, Gaussian, Most Positive and Most Negative Curvature. Each curvature attribute

includes a corresponding curvature azimuth volume that contains direction information of the curvature (Fig. 12).

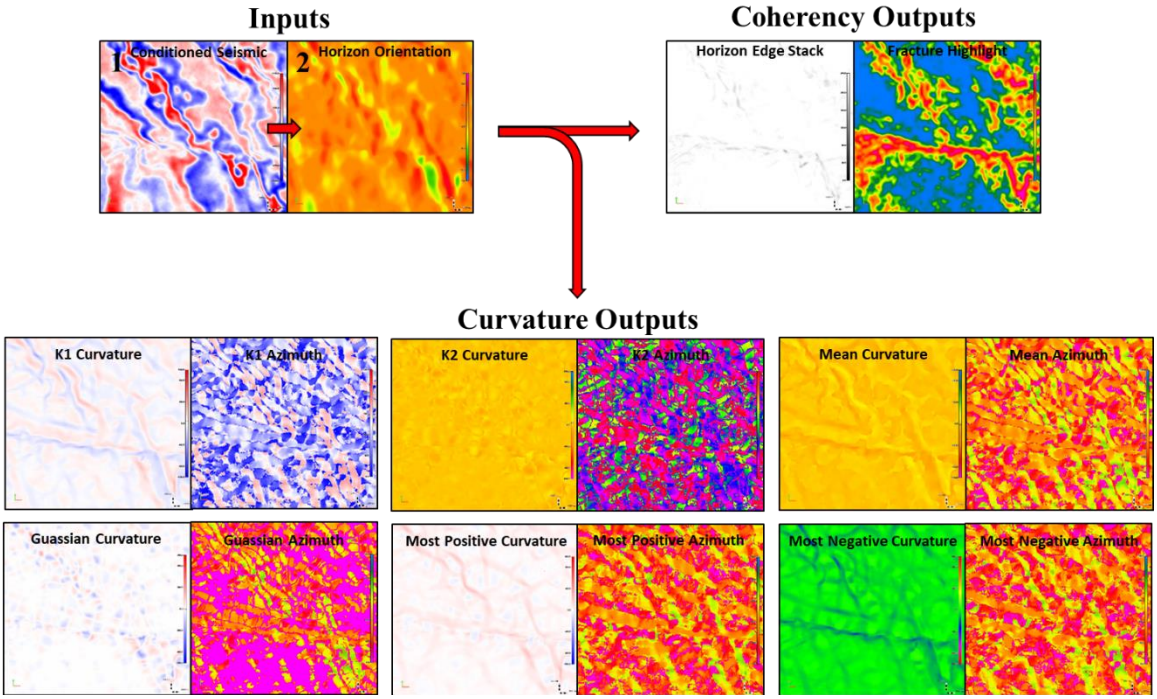

Figure 12: Shows the inputs for the coherency attributes (top right) and curvature attributes (bottom) all at 2000 ms. Both the Horizon Edge Stack attribute and the Fracture Highlight attribute are specially tuned for detecting fractures below naked eye resolution. Examples of the six curvature attributes, and their associated azimuth attributes, tuned specifically for fracture characterization including from left to right, top to bottom: K1, K1 Azimuth, K2, K2 Azimuth, Mean, Mean Azimuth, Gaussian, Gaussian Azimuth, Most Positive Curvature, Most Positive Azimuth, Most Negative Curvature, and Most Negative Azimuth.

3.3.6. Discrete Fracture Network

The last seismic fracture characterization step is generating a discrete three-dimensional fracture network (DFN), fracture vector glyphs, and interactive rose plot diagrams for fractures orientation. The DFN is generated in iterative processes through the following steps:

(1) The procedure starts with the conditioned volume, Horizon Orientation volume, and the Horizon Edge Stack attribute volume (Fig. 14a, 14b, and 14c respectively) as inputs to create a Strike Enhance attribute (Fig. 14d). The Strike Enhance attribute is a coherency

class attribute that has a corresponding Intermediate Strike volume containing fracture strike and dip information. The settings for this step are specifically designed to amplify fracture signatures as the base operator parameter was set to 2 traces in order to increase the measurement density to include smaller scale features, like fractures.

(2) Using the Horizon Edge Stack attribute volume, the Strike Enhance attribute volume, and the Intermediate volume as inputs, a Dip Enhance, another coherency class attribute, and a corresponding Intermediate Dip attribute, which contains additional refined fracture strike and dip information, were generated (Fig. 14e).

(3) The Horizon Edge Stack, Strike Enhance, Intermediate Strike, Dip Enhance, and Intermediate Dip are all used as inputs to generate a final, refined and superior Fracture Enhance, another coherency class attribute, and a Fracture Orientation attribute, which contains the final refined fracture strike and dip information (Fig. 14f).

(4) The next step was to extract the fracture cuts from the final Fracture Enhance and Fracture Orientation volumes to generate the DFN. Using these two attribute volumes as inputs, the Minimum Fault Cut Length, Cluster Size, and Minimum Connected Voxel (essentially a pixel) Value settings were all lowered in order to adequately extract the smaller scale fracture pointsets. At this point, the fracture pointsets were converted to fracture surfaces thus creating a 3-D DFN (Fig. 15).

(5) Interactive rose diagrams that contain fracture strike and dip orientation information were created to analyze the dominant fracture strike and dip orientations.

To add additional fracture information below the visibility of the naked eye, fracture vector glyphs were generated and displayed in the seismic volume and associated attributes (Fig. 15). Glyphs are essentially vectors that are an indication of the fractures. The direction of the Glyph is calculated from the Fracture Orientation attribute cubes, which represents the strike of the fault/fracture. The height and the length of the glyph is calculated from the fracture probability

cubes that were calculated in the background during the Fracture Enhance attributes process described in step 3. The longer and the thicker the Glyph, the higher the likelihood of fault/fracture occurrence (CGG-Geosoftare, 2015 and 2018).

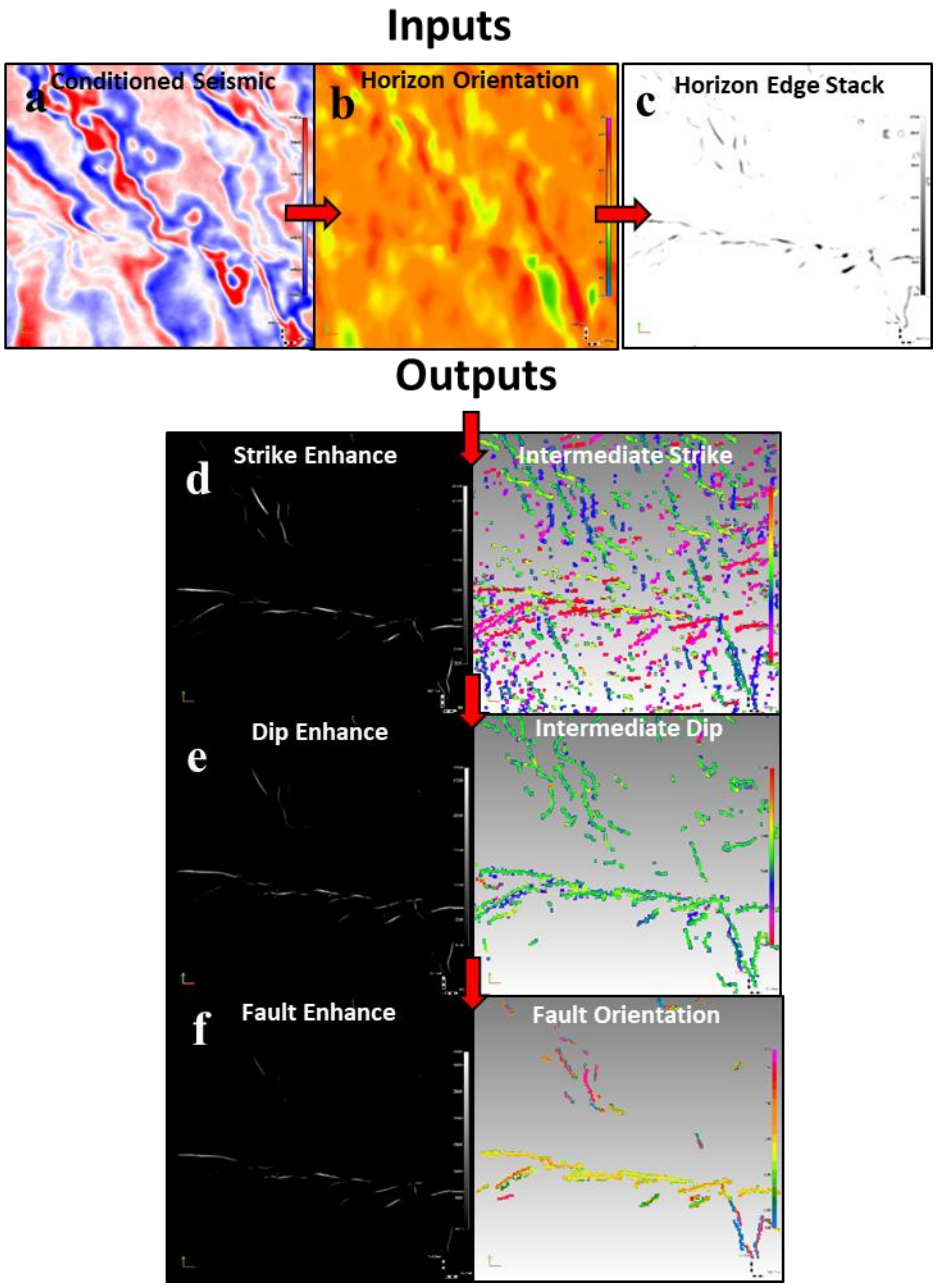

Figure 13: List of the attributes generated in an iterative process to be used as inputs for the DFN generation step. The conditioned volume, Horizon Orientation Volume, and Horizon Edge Stack Volume are used to generate a series of coherency attributes that are filtered from the Strike Enhance stage, to Dip Enhance, and finally the Fracture Enhance volume which minimizes noise and amplifies the fracture signal were used to generate the DFN.

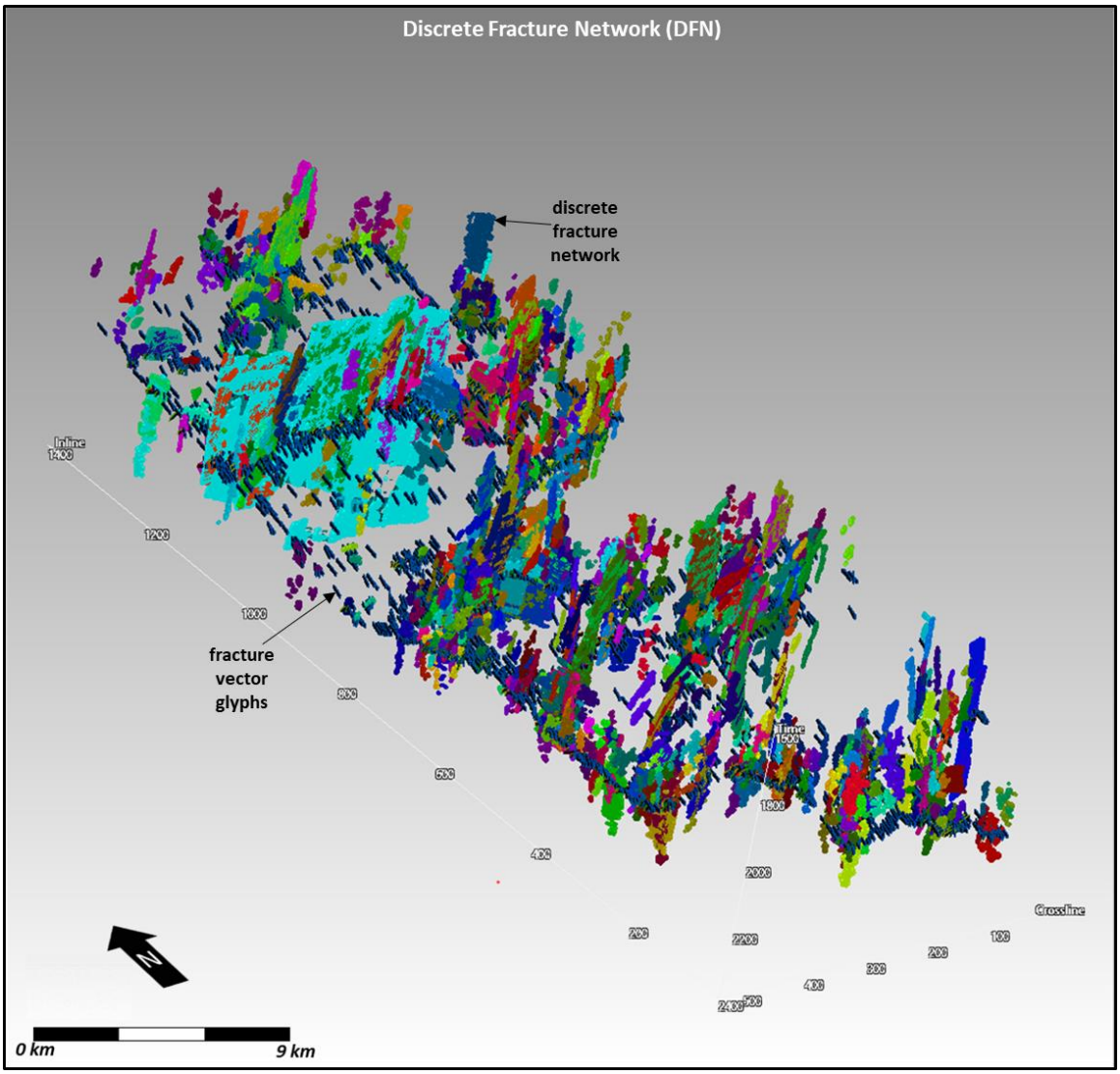

Figure 14: 3D view of the DFN showing all extracted fractures and the fracture vector glyphs. Interactive rose diagrams could subsequently be generated to show fracture orientation within specified intervals.

3.4. Petrophysical Analysis for Fracture Detection

The petrophysical evaluation added additional information about occurrence and density of fractures at the log scale. The petrophysical analyses were generated in conjunction with and supplied by NUTECH Energy, a service company that specializes in reservoir characterization. NUTECH provided their NULOOK natural fracture analysis petrophysical evaluation called

Fracture Intensity Vision (FIV). It is an advanced petrophysical model tuned specifically for detecting fractures, determining fracture probability, and relative fracture density. Using proprietary algorithms, FIV utilizes and compiles a series of natural fracture indicators such as "chattery" caliper logs, greater than normal compensation on density logs, various indicators from resistivity ratios, and compensated neutron density/sonic relationships to indicate the possibility and confidence level of a natural fracture at a given depth. When a number of these independent indicators occur at the same depth, the confidence of an existing natural fracture increases. When the confidence level is reached (2 indicators), a fracture intensity counter is used to accumulate the number of indicated fracture feet. Often times, the more indicated feet, the better the potential producibility of the interval (Hill, 2009). The wireline logs were also quality controlled and, in some cases, normalized or edited if noisy or ambiguous data existed.

The lateral investigation and vertical resolution of the fracture detection is variable and log dependent. For example, the vertical resolution range for all utilized logs are between 0.15-2.5 m (~0.5-8 ft) and the lateral depth of investigation ranges from cm's – 2.5 m. To clarify, the caliper log only gives an indication of fractures along the borehole, the density log measures several cm's (a few in's) into the formation, and the resistivity log measurements range from a 0.3-2.5 m (~1-8 ft) into the formation, the sonic log measures tens of cm's (~1 ft) into the formation. Due to the fact that different logs have varying resolutions and depth of investigations, this study just summarizes these differences and groups them in to "log-scale resolution" and compares the results in a relative sense. Regardless, fractures haven been shown to be detectable with any one of the mentioned logs if needed, but the confidence of the presence of fractures is increased by the detection of fractures from numerous logs which is what is done in this study (Hill, 2009).

3.5. Formation MicroImaging (FMI) Log Analysis for Fracture and Stress Evaluation

One of the most critical datasets for characterizing fractures was the FMI log from Well D provided by Devon Energy Corporation. Borehole image logs, or Formation MicroImaging (FMI) Logs are electronic pictures of the rocks and fluids encountered by a wellbore (Hurley, 2004). The electronic images were generated by microresistivity measurements in water-based mud yielding excellent image quality. A stable borehole results in a better image quality but also means less detailed information regarding the in-situ stress state. Borehole breakouts are thought to preferentially occur parallel to the minimum horizontal stress (σ_h) and orthogonal to the maximum horizontal stress (σ_H) (Barton et al., 1988; Barton et al., 1997; Barton et al., 1998; Fossen, 2010). The FMI log was interpreted manually in a foot-by-foot fashion from the top of the "Meramec" interval, through the "Osage" interval, and ending in the Woodford interval. Three measurements were compiled: (1) total relative length of fractures, (2) number of visible fractures, and (3) fracture orientation information (i.e., strike and dip).

Since the resolution of the FMI log is less than that of the core, only a relative fracture density and fracture length can be gathered. The number of fractures was determined by adding the total number of distinguishable separate fractures within a one-foot zone. For fracture length, this was done by measuring the vertical length of the fractures in a one-foot zone and adding the lengths when there was more than one fracture.

3.6. Core Description for Fracture Analysis

Two cores within the seismic survey area (Fig. 5) were made available for this study. The first core, which sampled the entire "Meramec and Osage" intervals, was located near the northwest corner of the survey (Fig. 5). The second core, which only sampled the basal ~6 meters

(20 feet) of the “Osage” interval was located in the northeast part of the survey (Fig. 5). The face of the core slabs were described in one-foot intervals in order to have a consistent, but still relative, comparison to the fractures characterized by the FMI log and petrophysical evaluations. Fracture dip was determined; however, fracture strike direction was not measured because the core was not oriented.

Similar to the FMI log analysis, it is challenging to differentiate between induced fractures created during the core extraction process, enhanced natural fractures, and unaltered natural fractures. Characterizing the type of fractures was done primarily by identifying the type of mineralization in the fractures. If the fractures were completely mineralized with calcite cement, then the fractures are most likely natural fractures (Kulander et al, 1990). If fractures were open, then they could be segregated as real or artificial fractures depending if there was mineralization present along the walls of the fracture. To ensure the mineralization was a mineral and not drilling mud, an attempt to smear this material was made to determine if it was moveable or not. When the material could be wiped away, it was obviously indicative of drilling mud. If the break was clean or had drilling mud in some places but had mineralization along the fracture walls in other places, it was determined to be a natural fracture that had been enhanced by the core extraction process.

Overall, most of the core was interpretable (Fig. 16a) but some portions of the core were severely damaged by the coring process resulting in near pulverized sections of rock (Fig. 16b). These zones were uninterpretable and not included in the analysis. The core results were compiled into fracture density curves and were compared to the relative fracture density curves extracted from the FMI log interpretation and the petrophysical evaluation. To accomplish this, the core depths had to first be registered to the log depths. This was accomplished by correlating the gamma ray from the wireline logs to the core gamma ray which was generated using a hand-held gamma-ray spectrometer device that measured gamma ray counts along the face of the core.

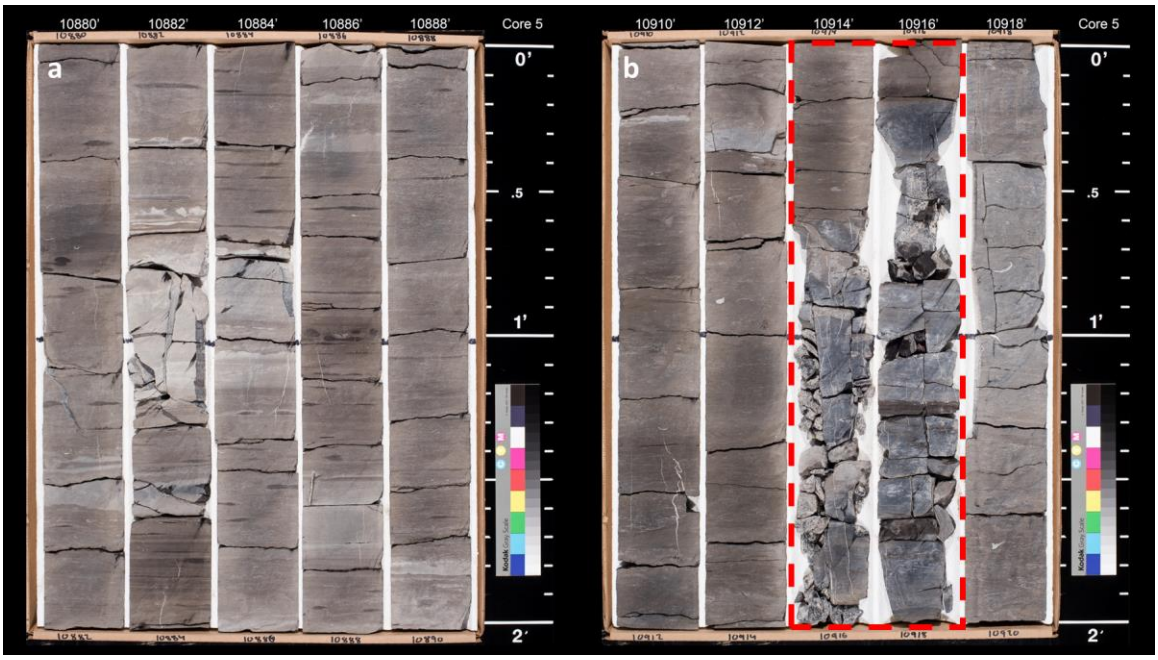

Figure 15: a) Interpretable core with fractures. b) Red dashed outline shows uninterpretable core that was damaged during the coring extraction process.

CHAPTER IV

DATA INTERPRETATION

4.1. Seismic Interpretation

The seismic data was interpreted mainly to characterize fractures, in-situ, and paleo-stress regimes at the seismic scale through: (1) building and interpreting a standard stratigraphic foundation, (2) establishing/interpreting a large-scale structural framework and finally (3) interpreting smaller scale fractures using a series of generated attributes and a discrete fracture network. Building the large-scale structural framework was critical in finding clues to the local in-situ and paleo-stress states and shed light on how associated structural features may be behaving. Identifying and interpreting large scale faults and other geologic features such as horsts and grabens was key in accomplishing this goal. Interpretation of the seismic data focused on the northern half of the survey, which contained all available well control that could act as a ground truth.

Establishing a basic stratigraphic horizon interpretation was a necessary step to ensure structural interpretations maintained geologic reasonableness and acted as a guide and reference to correlate interpretations from seismic to core. Horizons interpreted included the “Meramec,” “Osage,” Woodford, and Hunton. These horizons defined zones of interest and were used to understand the presence of fractures in each interval, especially the “Meramec and Osage” intervals.

The most dominant structural feature interpreted from the seismic data was a large oblique fault that appears to have left-lateral slip and is down thrown to the south with a vertical offset of ~75 meters along the fault (Fig. 17). Interpreting the fault as left-lateral based on offset seismic amplitudes and discontinuous horizons alone was extremely difficult and would have likely resulted in erroneous interpretations. Identification of several key geologic features along the fault was critical for confirming the movement direction and stress orientations required to cause such movement. First, two separate grabens and a horst feature were interpreted along what appeared to be the releasing bends and a restraining bend respectively along the large oblique fault indicating left-lateral movement (Fig. 17). The first graben is most easily seen in section view as shown in (Fig. 17a). A horst feature was identified along a restraining bend that would also indicate left-lateral movement (Fig. 17b). The second graben feature can also be identified in section view (Fig. 17c). Finally, A NW-SE striking fault was interpreted from the Most Negative Curvature attribute to be an older fault that had been offset to the left by the large E-W trending oblique fault (Fig. 18). This NW striking fault was interpreted to be an older fault for three main reasons: (1) its orientation was inconsistent with the vast majority of the interpreted faults and fractures. (2) It is laterally offset ~320 meters by the large ~E-W trending oblique fault. (3) The fault appeared to die out into the base of the "Osage" surface (~1750ms) while the large oblique fault projected all the way through ~1500 ms through the Pennsylvanian section. In other words, the vertical offset of the older fault progressively decreased from the Hunton to the base of the "Osage."

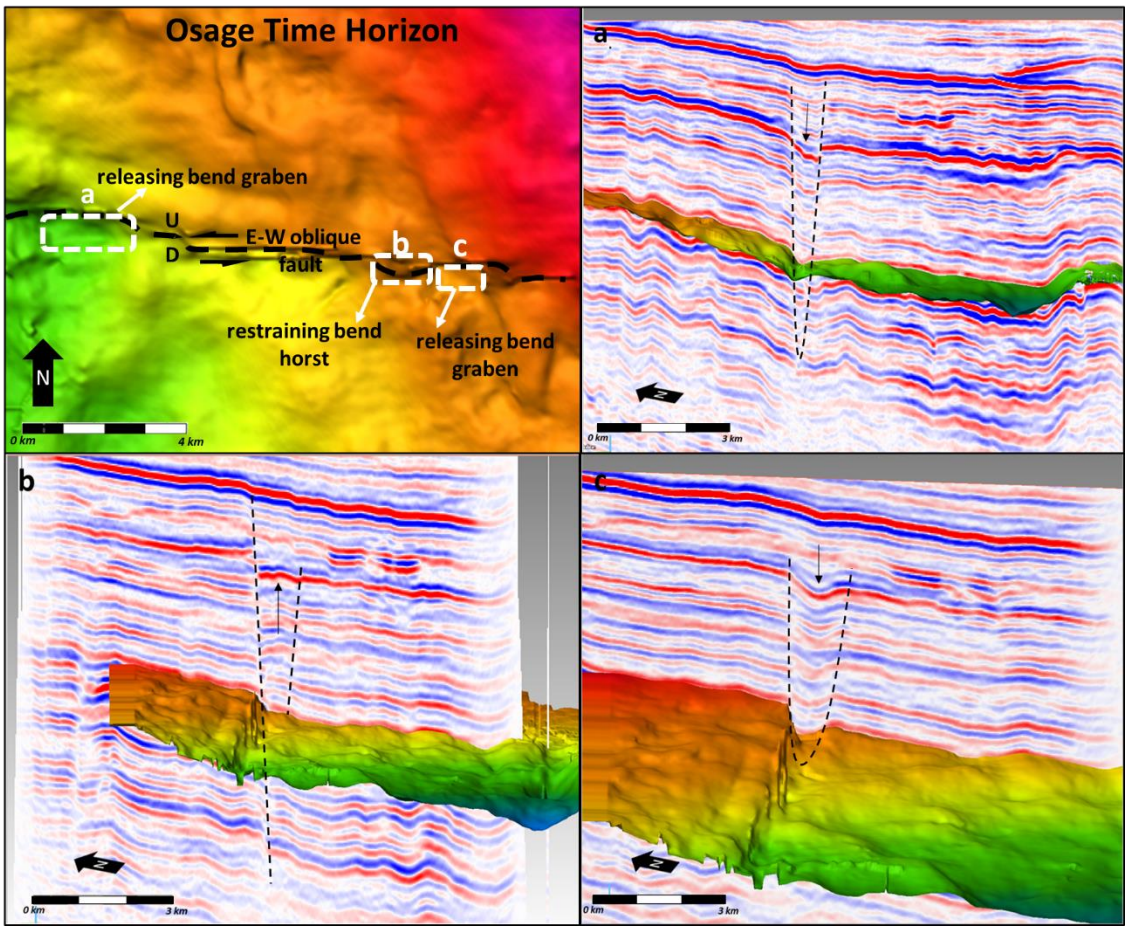

Figure 16: Top figure is the "Osage" time horizon, areas of interest are outlined in black dashes. a) interpreted horst feature along a restraining bend of the large oblique fault. b) An interpreted horst or half-graben along a restraining. c) Another graben along the releasing bend of the fault. All interpreted structural features indicate a left lateral movement along the E-W oblique fault.

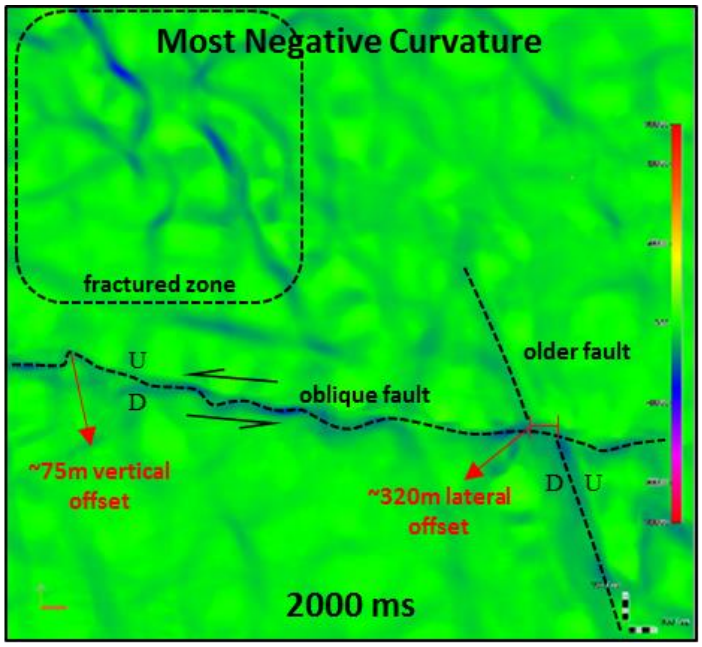

Figure 17: Most Negative Curvature attribute at 2000 ms showing the large left-lateral oblique fault near the north central portion of the survey. Dark blue areas show highest negative curvature. An interpreted older fault is also accurately imaged and shows offset to the left on the north side of the oblique fault. Another fractured zone was identified in the NW corner of the seismic example shown here and is later compared to the fractures from the image log in *Fracture Orientation 5.1* section.

The seismic interpretation and characterization of smaller scale fractures and zones that appeared to be highly fractured were completed through integrating a series of attributes, a DFN, fracture vector glyphs, and rose plots. All fracture detection techniques were fairly consistent and depicted the occurrence and nature of fractures. The curvature attributes including: K1, K2, Mean, Gaussian, Most Positive and Most Negative Curvature were generated to better visualize fractures. Of these, the most useful curvature attribute in this data set appeared to be the Most Negative curvature (Fig. 18). It best highlights the presence of fracturing and faulting along the approximately E-W trending large oblique fault. This was expected as often large-scale faults have numerous associated faults/fractures occur in close proximity. Additionally, it helped identify a fractured zone in the NW portion of seismic volume. Furthermore, it helped delineate the older NW-SW trending fault described earlier. The Fracture Highlight attribute identified heavily fractured zones and fractured zones that may have gone undetected to the naked eye.

There were some identifiable zones that appeared to be highly fractured without the presence of visually identifiable faults (Fig. 19).

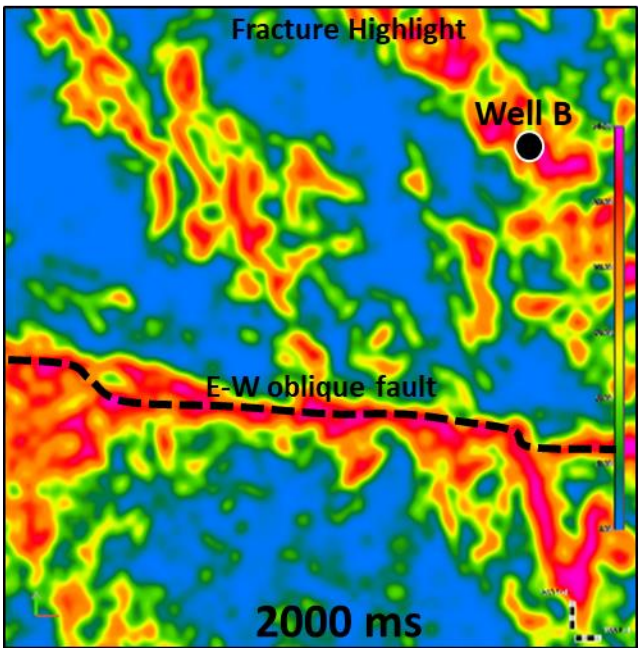

Figure 18: Fracture Highlight Attribute at 2000 ms. A fractured zone that didn't contained any extracted fault cut surfaces was identified near Well B. This is studied further in the *Fracture Density 5.2 section.*

The DFN gives the interpreter a visual three-dimensional view of the fracture network and displays visible fractures and smaller scale fractures that cannot be seen with the naked eye (Fig. 20a). Additionally, the generated interactive rose plots display fracture orientation information (Fig. 20a). Through the "Meramec and Osage" intervals, the dominant fracture dip orientation determined from seismic data was near vertical as the dip ranged between 75°- 90° and the strike was mainly NE-ENE (45°- 67.5°). The secondary fracture orientation was also near vertical but striking E-W (~90°). The generated fracture vector glyphs, which contain fracture orientation and confidence information (Fig. 20b) were useful in higher fracture density zones that had no significant visible fractures within the DFN. The vector glyphs indicated dominant fracture strike roughly in the NE direction. This greatly improved the ability to visualize smaller scale fractures undetectable to the naked eye and provided critical orientation information.

Output

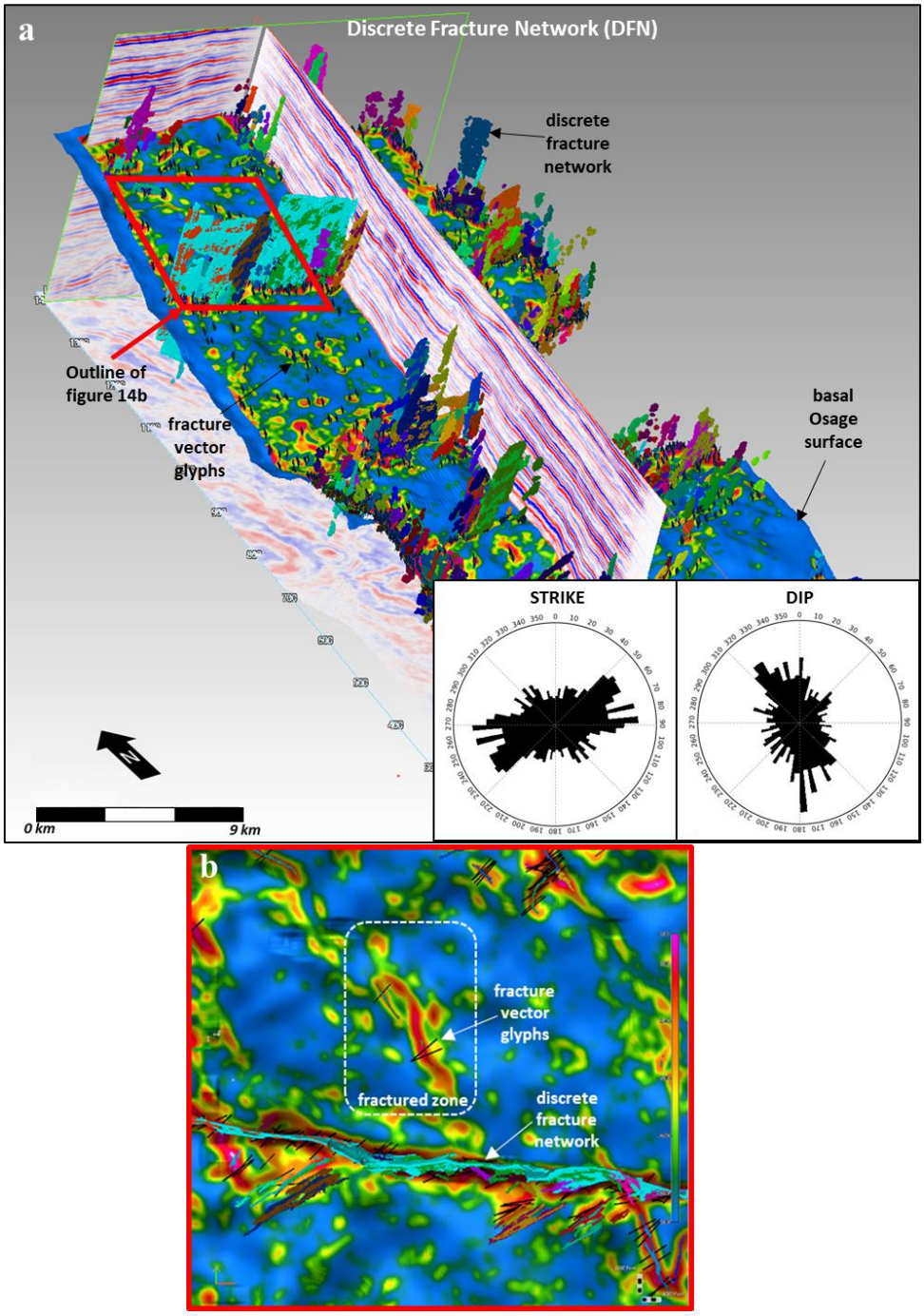

Figure 19: a) Discrete fracture network overlain the Osage horizon with a Fracture Highlight attribute, and strike and dip rose plots displaying fracture orientation. b) Close up of the Osage horizon co-rendered with the Fracture Highlight attribute and fracture vector glyphs. Figure illustrates how the fracture vector glyphs are useful in identified potential fracture zones and fracture orientations in scenarios where there are no discernable fractures to the naked eye.

4.2. Petrophysical Interpretation

The NULOOK FIV petrophysical evaluation was compeletd using a selected log suite from the six wells in the study area. The aim of the FIV analysis was primarily the detection of the presence of fractures, estimating fracture intensity, and drawing basic reservoir quality relationships related to fractures. Additionally, the petrophysical evaluation benefited from the other obtained log tracks such as gamma ray, caliper, porosity, a volumetric lithology track, bulk volume hydrocarbon and water, permeability, oil in place, and a reservoir quality flag track. The reservoir quality track is generated from tripped pay flags including the Reservoir Flag, Free Water Flag, Hydrocarbon Flag, Fair Permeability Flag, and the Good Permeability Flag. The thresholds and parameters of each of these flags is shown in Figure 21. The reservoir quality is broken down into four categories: non-reservoir (no flags), fair reservoir (e.g. 3 pay flags), medium reservoir (e.g. 4 pay flags), and good reservoir (e.g. 5 pay flags). All available curves were used to constrain and bolster fracture interpretations. Both "Meramec and Osage" intervals contained log detected fractures, but a few traits persisted for each interval. The "Meramec" was much less prone to fracturing when compared to the "Osage" interval. Over the six wells, the average FIV estimated fracture length per foot in the "Meramec" interval was 0.045 ft while the average fracture length per foot in the "Osage" was 0.115, which is a 155% increase of fracture length per foot.

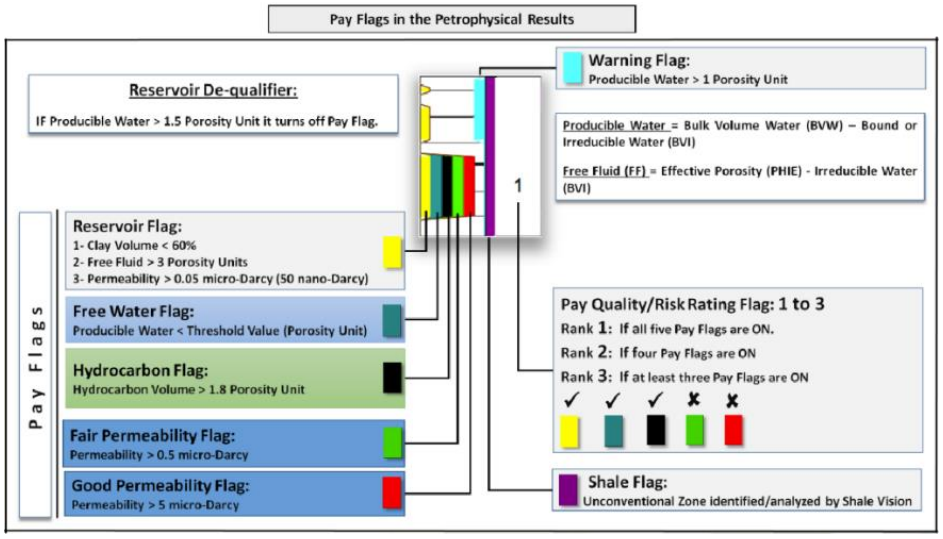

Figure 20: A chart describing the PAY track included in the NUTECH FIV analysis which contains reservoir quality flag indicators and their associated triggering thresholds (modified from Nutech, 2018)

In most cases, fractures preferentially occurred in calcite rich zones for both intervals, but their effects on reservoir quality were very different for the "Meramec and Osage" intervals. For example, in the "Meramec" interval, in all six wells, there was a slight positive correlation between the increase in porosity and permeability with the presence of fractures. However, there appeared to be a very strong negative correlation between reservoir quality and increasing calcite content in the "Meramec" interval (Fig. 22). This indicated that fractures only benefited the overall reservoir quality in the "Meramec" interval when they occurred in more quartz rich zones, which was very rare compared to when they occurred in zones that had an increase calcite content. The "Meramec" interval overall contained better reservoir quality compared to the "Osage" and ranged from non-reservoir to good reservoir quality. The upper "Meramec" zone typically contained the thickest and best reservoir intervals. Alternatively, in the "Osage" interval, fractures, for the most part, positively affected reservoir quality regardless of mineralogy. As a whole, the "Osage" interval was an inferior reservoir ranging from non-reservoir to medium

reservoir quality. Medium quality reservoir in the "Osage" was rarely achieved without the influence of fractures though (Fig. 23).

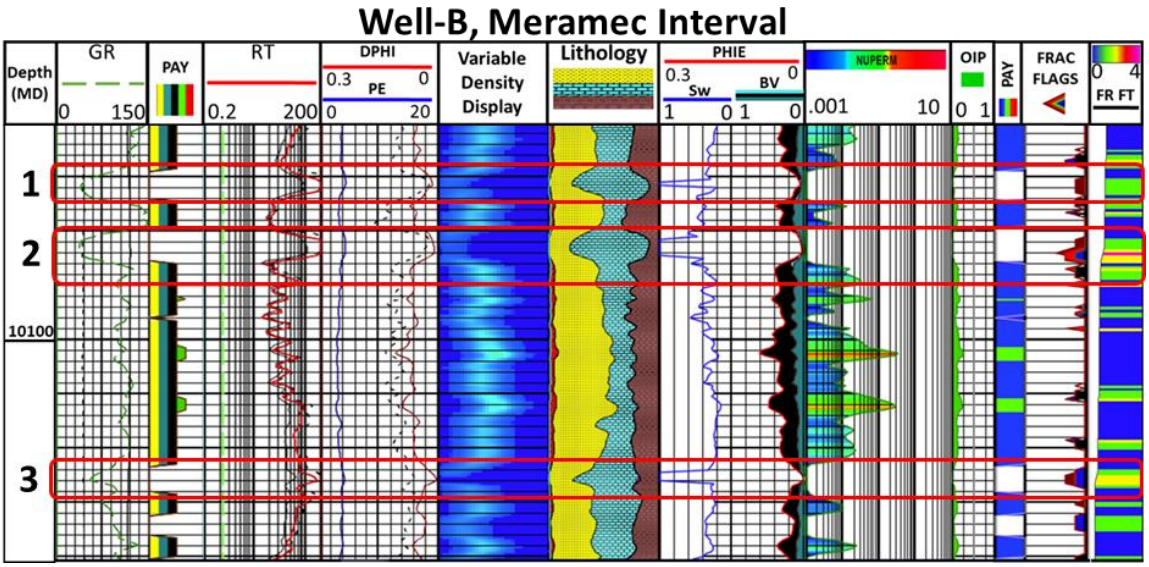

Figure 21: NULOOK FIV evaluation of Well B in the "Meramec" interval. Zones outlined in red show highly fractured zones (indicated by the "FRAC FLAGS" and Fracture Feet (FR) tracks on the far right) have an overall increase calcite content and lower permeability compared to less fractured surrounding zones. In the "Meramec" interval, better reservoir quality (see "PAY" track is associated with less calcite content and less fracturing.

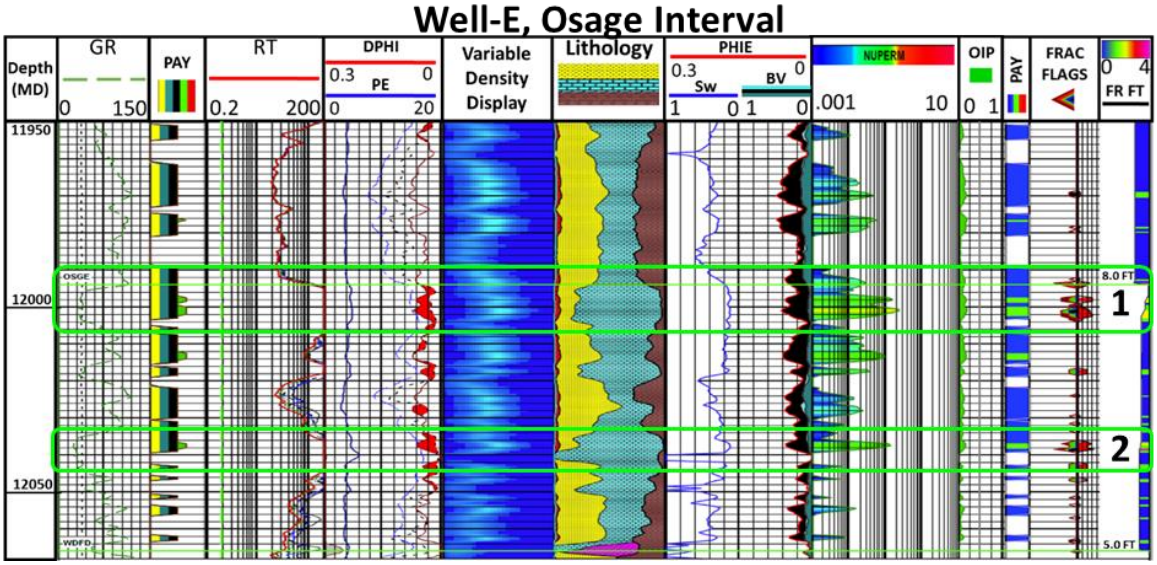

Figure 22: NULOOK FIV evaluation in the Osage interval in Well E. The zones outlined in green show that the best reservoir quality often occurs in highly fractured zones.

4.3. FMI Log Interpretation

Fracture characterization from the FMI log interpretation were essential to establish fracture relationships between the seismic-scale fractures and log-scale fractures. Establishing the quality and validity of the FMI log was important before interpreting geologic features such as fractures. The borehole appeared to be quite stable as the caliper log indicated a continually decreasing hole size from the "Meramec" through the Woodford and no borehole breakouts were visual on the FMI log. The "Meramec and Osage" intervals were interpreted for the occurrence, density, and orientation of fractures. The dominant natural fracture orientation interpreted in all zones was consistent and roughly oriented ENE (~67.5°). The secondary fracture orientation determined was oriented approximately E-W (~90°). Most interpretable fractures were near vertical (75°-90°) and appeared to be mineralized (Fig. 24) based on high resistivities. There were numerous noted induced fractures that were segregated from real fractures and subsequently interpreted. All induced fractures were roughly oriented E-W which is an indication of the in-situ σ_H direction (Fig. 25) (Barton et al., 1988; Barton et al., 1997; Barton et al., 1998).

All interpreted natural fractures from the FMI log were counted and measured on a foot-by-foot basis and then a "total number of fractures" curve and a "frac length" curve were generated. Observable fracturing trends are consistent with the petrophysical interpretations. In general, fracturing increases in more calcite rich intervals which is shown in Figure 26. There is a significant increase in fractures in the more calcareous rich basal "Meramec" interval and the "Osage" interval.

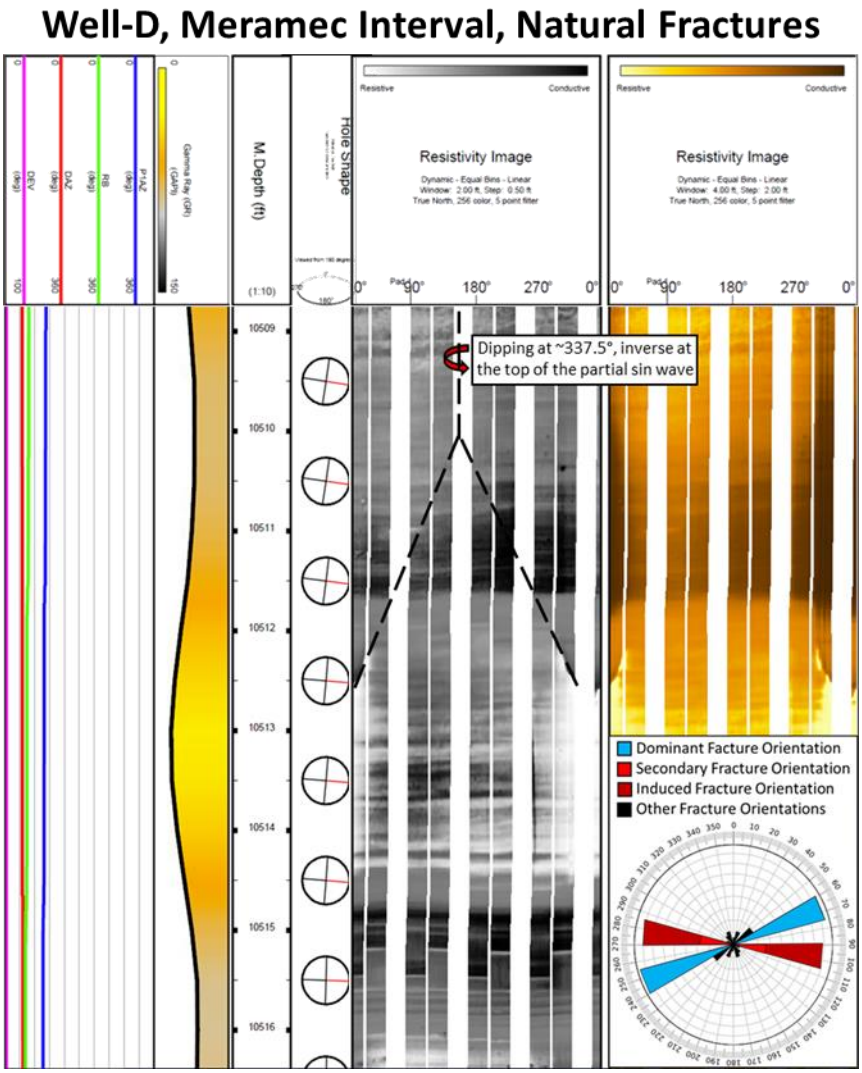

Figure 23: Interpreted fractures in FMI log within the "Meramec" interval from Well D showing natural fractures oriented ENE and E-W, which is consistent with the seismically detected fractures.

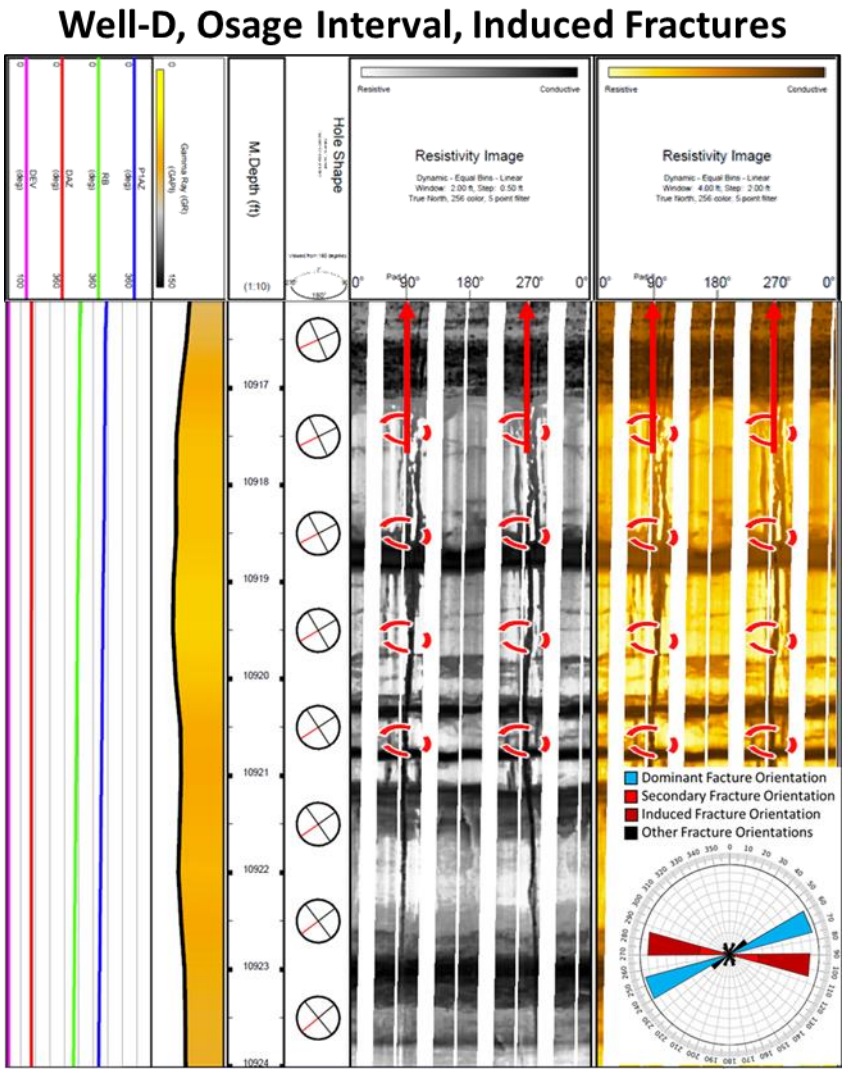

Figure 24: Interpreted FMI log showing drilling induced fractures oriented roughly E-W.

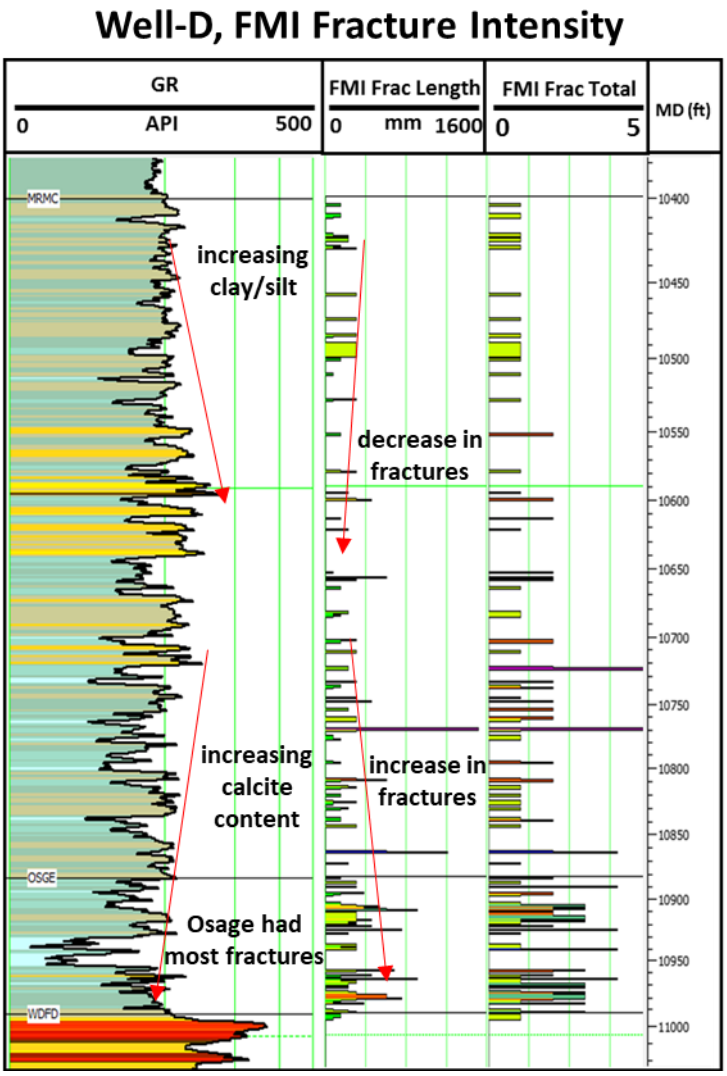

Figure 25: Fracture curves shown in tracks 2 and 3. A clear correlation of increased calcite content is consistent with increasing fracturing.

4.4. Core Interpretation

Two cores, from Well D and Well B, were interpreted for fractures in the "Meramec and Osage" intervals. Fractures in both cores showed similar characteristics such as orientation and preferred occurrence in calcite rich intervals but because the cores were not oriented, fracture strike was unobtainable. The vast majority of interpretable fractures appeared to be fully mineralized and near vertical (Fig. 27). However, investigation of the high definition ultra-violate (UV) and white light core images available from Well D, contained fractures which appeared to be fully mineralized to the naked eye but showed light-oil/condensate blue/yellow hydrocarbon fluorescence (Fig. 28). Zones that were more calcite rich, typically contained more fractures. Often, natural fractures and induced fractures coalesced in these zones together, requiring them to be segregated from each other. This was done by the identification of diagenetic cement or drilling mud along the fracture walls. For both cores, a relative fracture density curve was generated to compare with the FMI log and the seismic interpretations. The "Meramec" interval contained numerous interpretable fractures, but fracturing was only significant near the base of the "Meramec" interval. Alternatively, the "Osage" interval was much more prone to fracturing and fractures were evident in most areas of the core. The fracture density curves from both cores showed a significant increase in fracturing in the "Osage" interval relative to most of the "Meramec" interval (Fig. 30).

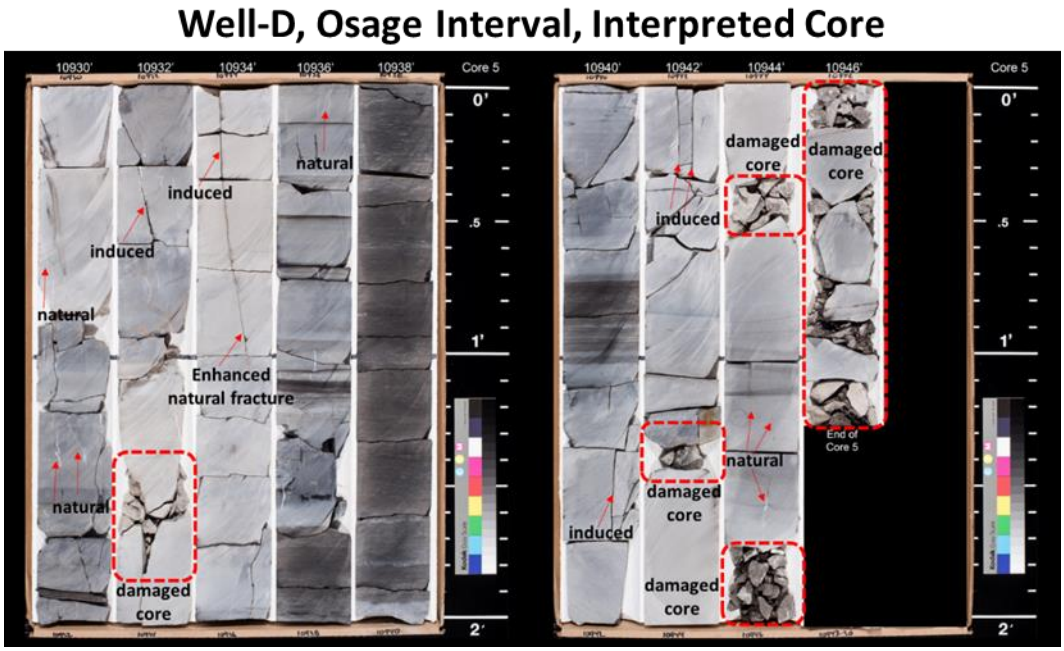

Figure 26: Core from Well D in the "Osage" interval. Red arrows point to natural, enhanced, and induced fractures. Red dashed outlines show areas where the core has been damaged. Natural fractures and enhanced fractures tended to coalesce in calcite rich intervals as shown here.

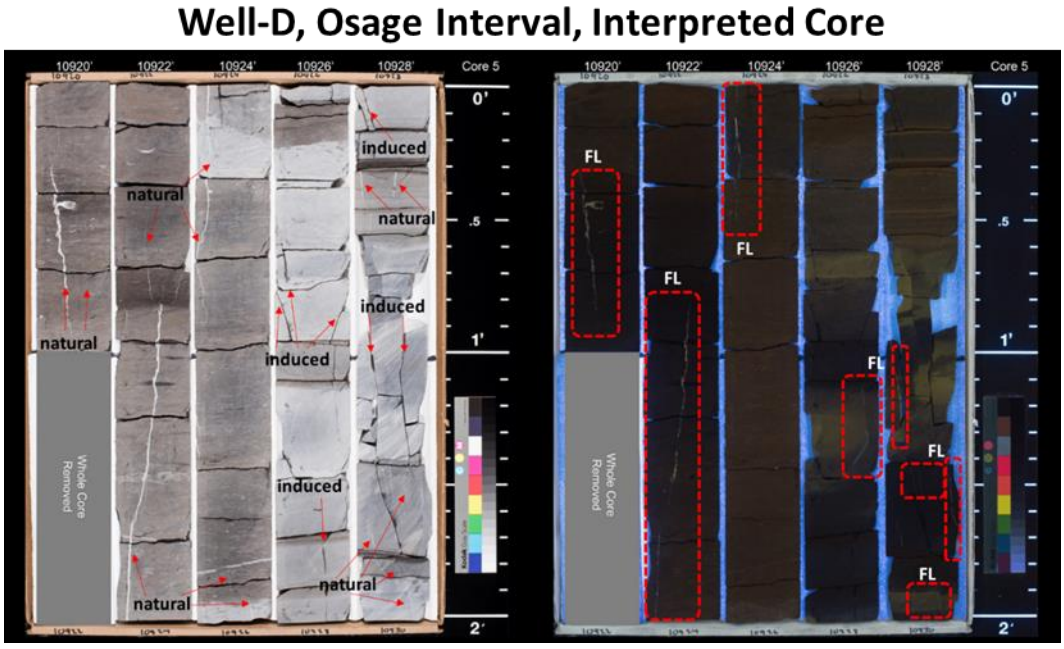

Figure 27: Left: HD white light core photo from the "Osage" interval from Well D. Natural and induced fractures appear to be fully mineralized with calcite cement. Right: corresponding HD UV light core photo showing light blue to yellow light-oil/condensate hydrocarbon fluorescence along the seemingly fully mineralized fractures. FL=fluorescence.

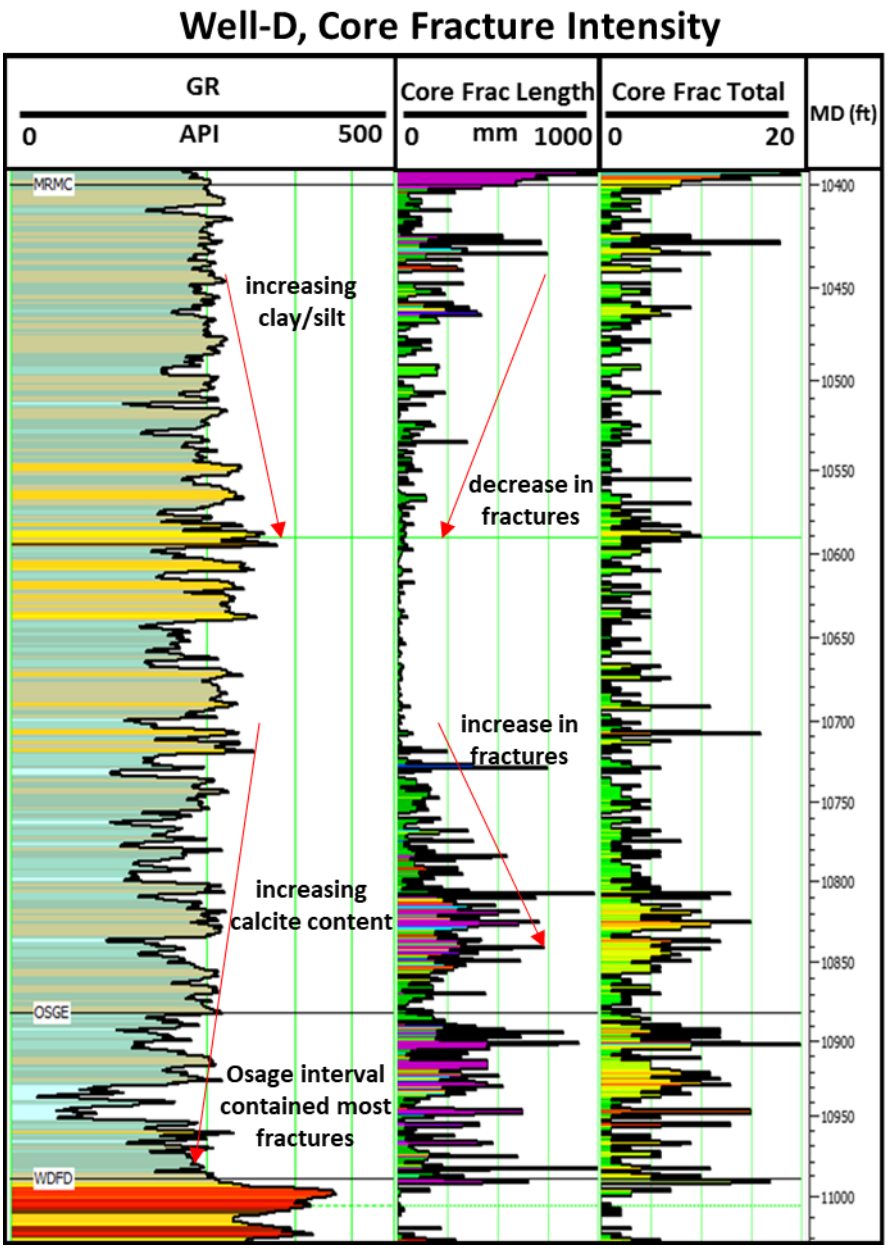

Figure 28: Core registered wireline gamma ray and core gamma ray (GR) from Well D are shown in tracks 1 and 2 respectively. Fracture length and total number of fractures interpreted from the core description are shown in tracks 3 and 4 respectively. An increase in fractures is shown starting in the lower "Meramec" interval and is maintained through the Osage interval.

CHAPTER V

DATA INTEGRATION

The integration of the datasets in this study aimed to draw fracture relationships at different scales. This chapter provides a detailed explanation of how the results of the different datasets were compared and integrated. First, it must be clearly understood that the scale of detected fractures is different based on the utilized dataset. However, comparing the density and orientations of fractures detected by the different techniques is necessary. The results of the in-situ and paleo-stress regime estimations will be also compared and integrated.

5.1. Fracture Orientation

Two datasets contained interpretable fracture orientation information, the seismic volume and the FMI log. The interpretations of both datasets were consistent in terms of the dominate and secondary fracture orientations which were roughly NE-ENE and E respectively. An example from only the seismically detected fractures around Well D is shown in Figure 32. Based off the DFN, interactive rose plots, and fracture vector glyphs created in the seismic interpretation workflow, the dominant fracture dip orientation determined from seismic was near vertical and ranged between 75°-90°. The dominant fracture strike orientation ranged between NE-ENE (45°-67.5°) (Fig. 32). The secondary fracture orientation was also near vertical but striking E-W (~90°). The dominant fracture orientation interpreted from the FMI log was also roughly ENE (~67.5°) with the secondary orientation being E-W (~90°) (Fig. 31). This indicated large scale seismically detected fractures were intrinsically related to smaller core/log scale fractures

interpreted from the FMI log, which matches an earlier finding by Butler et al., (1976) at Buchan field in the North Sea.

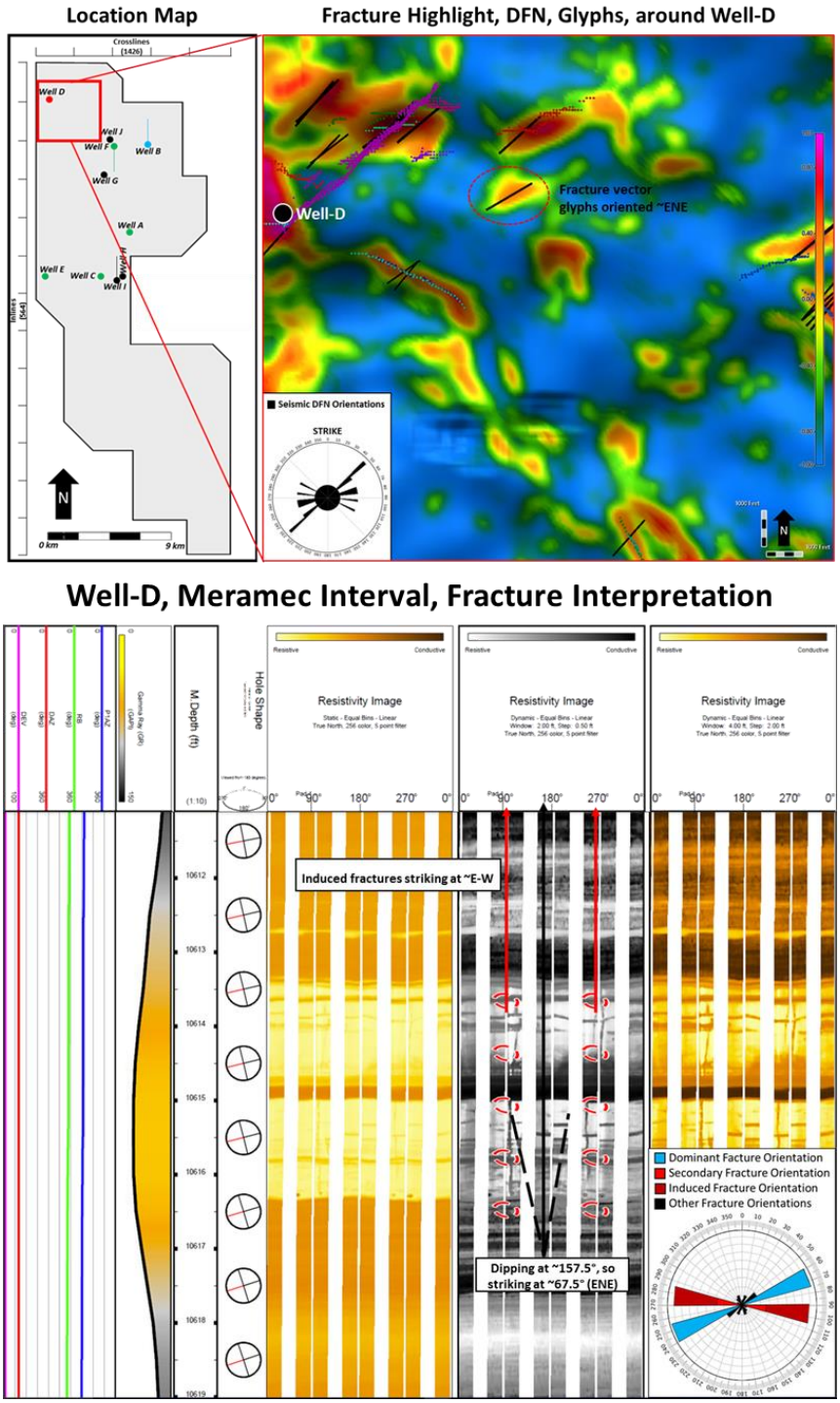

Figure 29: Fractures density and orientation around Well D from the seismic DFN, fracture vector glyphs, and seismic attributes (top panel). Fracture characterization from FMI log in Well D showing natural and induced fracture orientation (bottom panel). The seismic and FMI log results indicate a dominant NE to ENE and a secondary orientation of E-W.

5.2. Fracture Density

All available datasets (seismic, petrophysical logs, FMI logs, and cores) provided information about fracture density. Since different data sets characterized different scales of fractures, only relative comparisons were made between the densities of detected fractures from all the data. For example, core described fracture density curves were generated and compared to fracture intensity curves from the FIV petrophysical evaluations. The challenge was that the vertical resolution of the FIV log is significantly less than that of the core descriptions while the lateral depth of investigation for the FIV analysis is significantly more than the core descriptions. This has resulted in: 1) more fractures detected in core than that of the interpreted FIV analyses, 2) some fractures detected by the FIV were deeper into the formation and not visually evident in core, which limited the use of the core as "ground truth." However, if the fracture density curves showed to be relatively consistent in each dataset, then this confirmed a valid fracture density interpretation at two different scales. Once these interpretations were deemed relatively consistent, then they were compared to the FMI log interpretations to constrain both the core and FIV analyses.

Due to its vertical resolution being significantly less than that of core, and its lateral depth of investigation significantly less than the FIV analysis, the FMI log was most useful as a visual aid to quality control the FIV and core interpretations. The FIV analysis detected fractures several feet into the formation while the core and FMI log described fractures are interpreted along the wall of the borehole or the face of slabbed core. Still the two analyses were compared to see if a relative consistent interpretation was made. For the most part, the interpretations were validated, but there were several instances where discrepancies existed. This provided an additional quality control for the interpreted fractures and to also delineate real versus drilling induced fractures that the FIV may have incorrectly indicated as a natural fracture. Most of these inconsistencies were

the result of the FIV detecting what appeared to be drilling induced fractured as confirmed with the image log and core (Fig. 33).

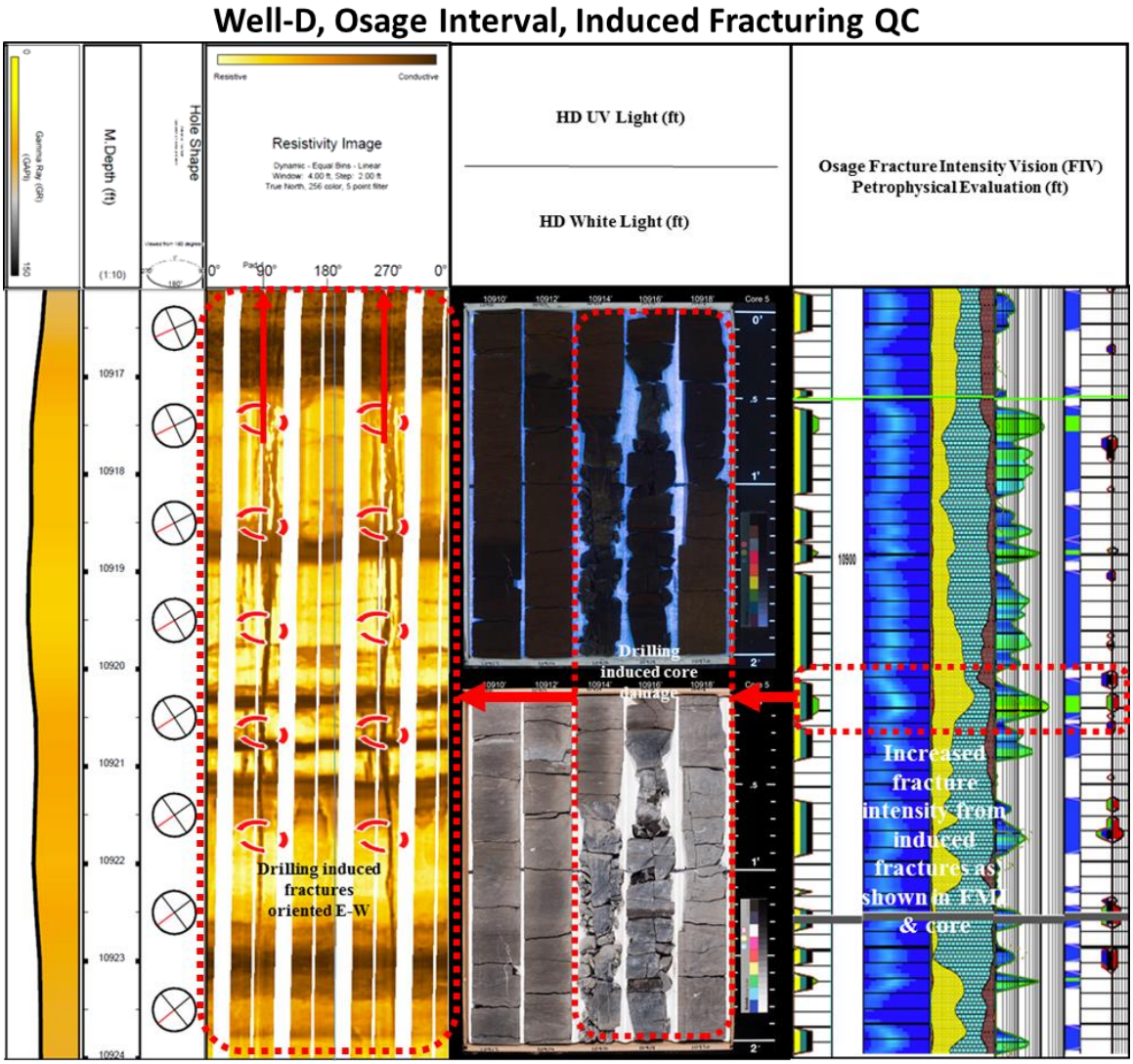

Figure 30: Well D induced fractures QC'd within the Osage Interval. Track 1: interpreted FMI log from Well D in the Osage interval, showing drilling induced fractures oriented E-W. Track 2: High definition ultra violet light and white light image core of the same section of core. Red dashed outlines core damaged from drilling and corresponds to the fractured zone identified in track 1. Track 3: Fracture Intensity Vision (FIV) petrophysical analysis over the "Osage" interval – red dashed outlined zone corresponds to the fractured zone identified in the FMI log.

The final and most challenging dataset to make relative fracture density comparisons to was the seismic volume. The resolvable seismic limit was determined to be 18-23 m (60-75 feet) within the intervals of interest. Researchers have obtained as good as 1/25 lambda for a detectable, not resolvable, vertical limit (Dorn, 2018). This would result in a vertical detectable limit, or visibility limit of 2.8-3.5 m (9.6-12 feet) for this survey. To simplify this challenge, the fracture density detected using the FIV petrophysical evaluation of both the "Meramec and Osage" intervals were compared to the interpreted equivalent zones as defined by the seismic well tie. This results in a bulk relative comparison. The well with the highest fracture intensity and the well with the lowest fracture intensity, based on the FIV analysis, were compared to the seismic data. Well C and Well B were chosen for this evaluation because they both contained an FIV analysis and demonstrated the highest (0.095) and lowest (0.022) fracture feet per vertical foot in the "Meramec and Osage" intervals respectively. Unfortunately, Well D, which also contained the FMI log, was not used for this interpretation as it is located near the edge of the seismic survey where the seismic signal/noise ratio is significantly low. Overall, there were fair visual correlations between higher fracture density and lower fracture density zones from the seismic attributes and FIV fracture intensity for both Well C and the Well B (Figs. 34 and 35).

Well-C fracture intensity from FIV analysis compared to seismic fracture highlight attribute.

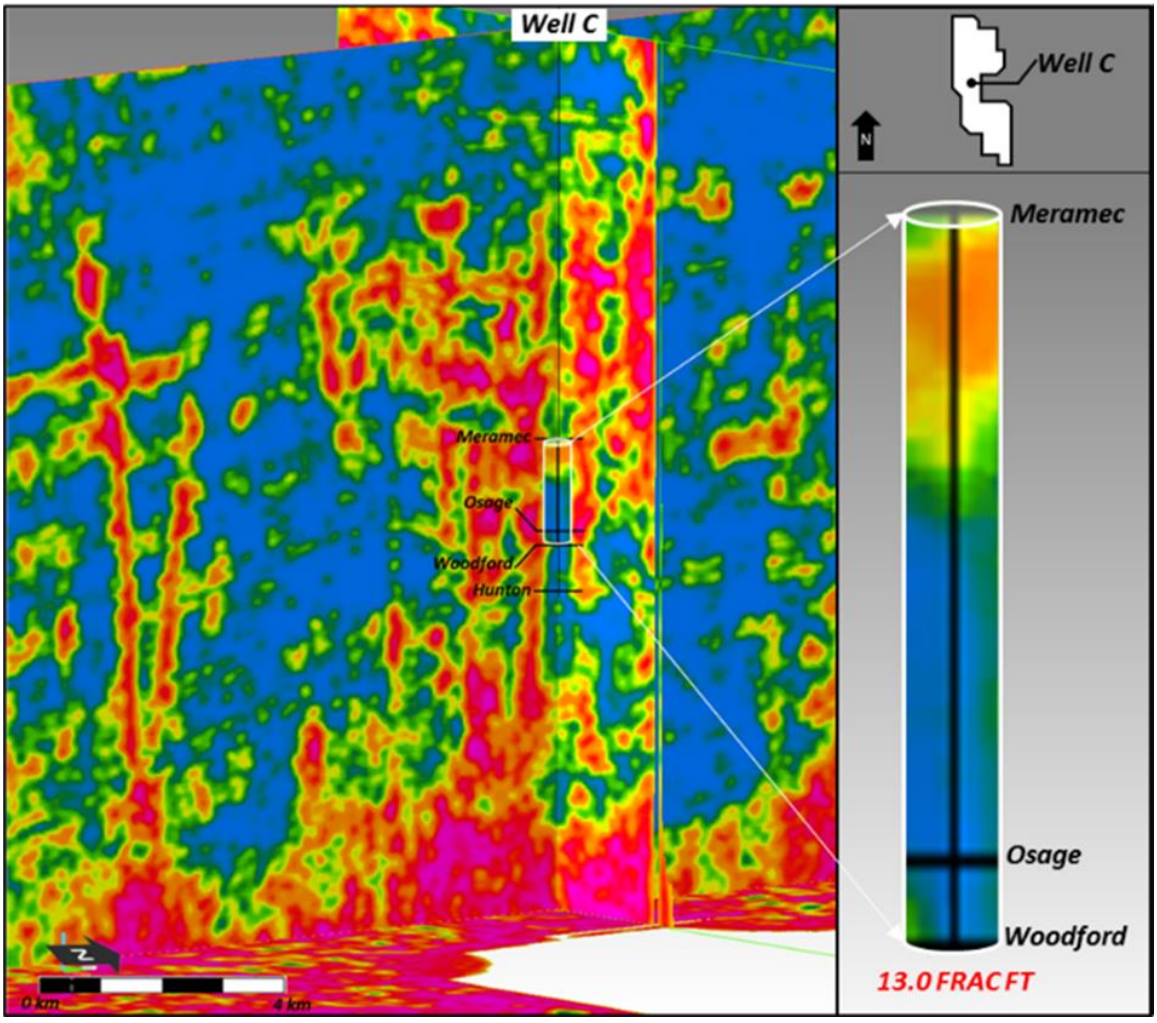

Figure 31: Shows the seismic Fracture Highlight attribute over the "Meramec and Osage" intervals at Well C. Right: figure shows seismic Fracture Highlight attribute over the "Meramec and Osage" intervals at Well C. Reds and pinks indicate higher fracturing. In the "Meramec and Osage" intervals, Well C contained 13.0 FRAC FT as estimated by the FIV analysis. Well B contained 53.0 FRAC FT over the same intervals. An obvious visual correlation is shown between higher FRAC FT corresponds to higher fracture density as shown in the Fracture Highlight attribute.

Well-B fracture intensity from FIV analysis compared to seismic fracture highlight attribute.

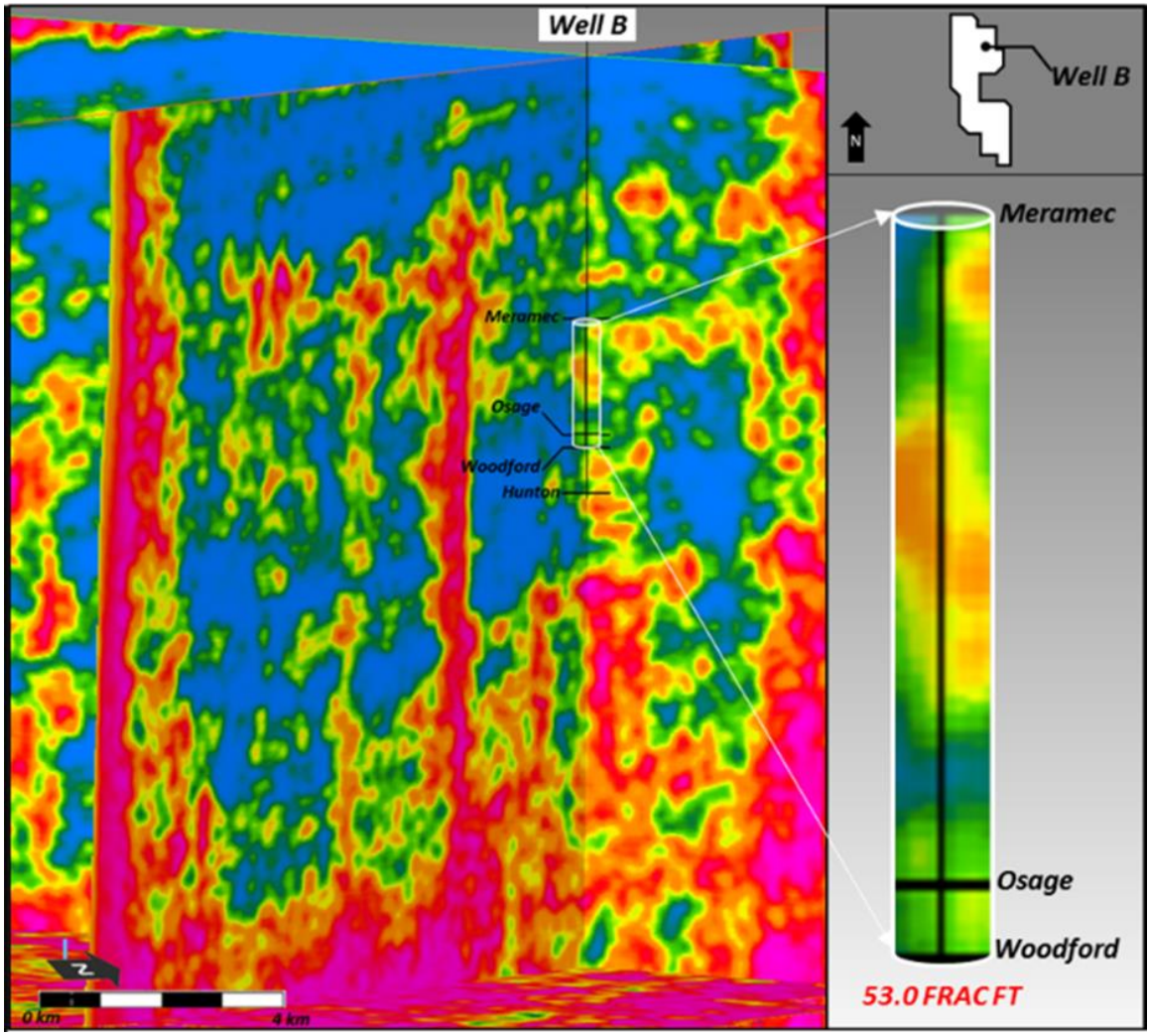

Figure 32: Shows the seismic Fracture Highlight attribute over the "Meramec and Osage" intervals at Well B. Right: figure shows seismic Fracture Highlight attribute over the "Meramec and Osage" intervals at Well B. Reds and pinks indicate higher fracturing. In the "Meramec and Osage" intervals, Well C contained 13.0 FRAC FT as estimated by the FIV analysis. Well B contained 53.0 FRAC FT over the same intervals. An obvious visual correlation is shown between higher FRAC FT corresponds to higher fracture density as shown in the Fracture Highlight attribute.

5.3. Stress Regime Evaluation

Three datasets were interpreted to provide in-situ and paleo-stress information within the study area: seismic, FMI log, and core. The interpreted seismic volumes contained several key pieces of evidence of in-situ and paleo-stress information in which several different interpretations were made. First, a large left-lateral oblique E-W trending fault which was down thrown to the south and propagated from the basement up into the upper Pennsylvanian strata was analyzed. This fault may have been reactivated and expanded during the Pennsylvanian. This indicates that at least during the Pennsylvanian, σ_H may have been oriented E-W. When combined with the FMI log interpretations that showed drilling induced fractures (parallel to σ_H) also occur E-W. This suggests that the dominant E-W σ_H orientation from Pennsylvanian times may have persisted to the present in-situ stress state. Second, within "Meramec and Osage" intervals, the dominant orientation of the seismically characterized fractures is NE-ENE, excluding the large E-W oblique fault. These detected fractures are thought to be older Mississippian extension fractures created from a previous stress regime with σ_H oriented NE-ENE. The dominant orientation of the fracture relative to the main oblique fault, which may have been active during that time, suggests that these fractures may fall under the T-fracture criteria (e.g., extension fractures 30°-45° from the main sense of slip). In either case, the culmination of these pieces of evidence indicates a simple shear structural deformation model (Fig. 36a) with an in-situ σ_H orientation being E-W that may have persisted from the Pennsylvanian to the present day while the σ_H was oriented NE-ENE during the Mississippian time (Fig. 36b). Another notable set of fractures occurred within the Hunton interval (Silurian age) were oriented ~NW (Fig. 36b). One of these fractures was shown to be offset by the large E-W trending oblique fault, shown in Figure 18, indicating it was from a separate older stress regime, likely Silurian in age. The interpreted fractures from seismic and FMI log show similar orientation (Fig. 34b). The

interpreted data in this study illustrates the possibility of reasonably identifying evidence for the rotation of σ_H orientations from ancient stress regimes to the present day in-situ stress regimes.

Additionally, the fractures described from the cores, although unoriented, act as validation to the FMI log interpretation as the cores were the only "hard" data set to confirm the presence of fractures. Since lateral depth of investigation of the core and FMI log are very similar, the fractures from each interpretation are likely similar once registered to the proper depth. Additionally, the majority of the fractures in core and FMI log were interpreted as extension fractures as they appeared to be mostly mineralized with no visible offset. The orientation characteristics of natural and induced fractures as interpreted from the FMI and core interpretations was consistent with the simple shear structural deformation model and the E-W σ_H orientation interpreted from the seismic data.

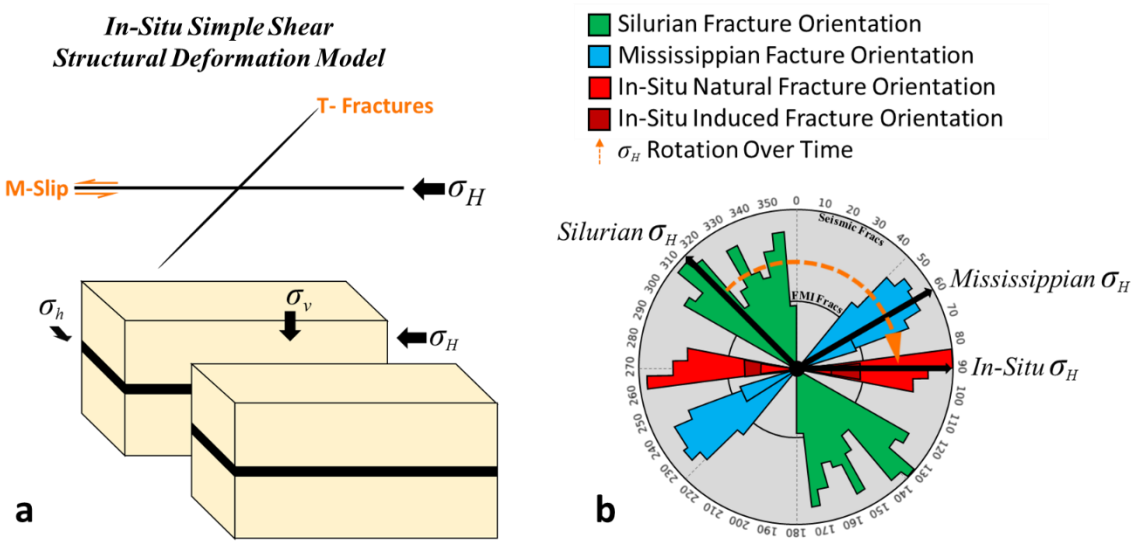

Figure 33: a) schematic illustrating the in-situ simple shear model and σ_H, σ_h, *and* σ_v orientations. b) Rose diagram illustrating σ_H rotations over time from the Silurian to the present based on fractures interpreted from both seismic and FMI datasets.

CHAPTER VI

DISCUSSION AND CONCLUSIONS

6.1. Discussion

Fracture characterization and the stress-state of unconventional oil and gas fields is often critical to the success of all phases of development including: exploration, drilling, hydraulic stimulation, and production. Typically, information about fractures and stress-states are derived from one type of data, which may lead to serious misinterpretations of a given reservoir or geologic feature (Hesthammer et al., 2001). This study illustrates how diverse datasets of different scales and resolutions can be integrated to generate a superior fracture and stress characterization. Often, the different data types overlap in scale allowing for an excellent quality control measure to strengthen the confidence of the interpretation. In other cases, the scales may not overlap but the features described in each dataset may have intrinsic and inherent geologic relationships, so relationships can still be drawn as long as the interpreter is aware of the limitations of each data type. Both of these scenarios were presented in this study and each acted as a "ground truthing" mechanism to either confirm an observation or identify possible sources of error.

Perhaps the most useful datasets in this study appeared to be the seismic and the FMI log as they were the only two datasets that provided both fracture density and orientation information. Interpreting fracture information from the seismic was a challenge as the data had to be heavily pre-conditioned to amplify real fractures while minimizing noise and artifacts. The majority of

the seismically interpreted fractures (real or artificial) were identified and segregated using the interactive rose diagrams to describe their orientation at different strike or dip directions. A preliminary understanding of the potential orientation of the fractures was useful in constraining the interpretation and investigating fractures with anomalous orientations. Fractures interpreted at the edges of the seismic surveys did not attain enough confidence due to the poor quality of the data near the survey edges and were removed from the seismic volume.

Fractures interpretation from the FMI log encountered several challenges that may have resulted in inaccurate FMI fracture orientation interpretations. These challenges included the possibility of the log measurement pads not having adequately sampled vertical and near-vertical fractures, which may have occurred in this study as the majority of fractures were mostly vertical. Possible variations in the nature of fractures even within the several centimeters between the two opposite walls of the borehole was also a problem. Additionally, possible millimeter-scale vertical and lateral lithologic variability may have significantly influenced the propagation or termination of fractures (Wang et al. 2019). In highly fractured zones, the FMI results showed numerous fractures that appeared to be identical or very similar in nature to another corresponding fracture.

Another FMI log interpretation challenge was the presence of drilling-induced or artificial fractures. In this study, artificial fractures were noticeably more conductive, had significantly wider apertures, were much longer, propagated through bed boundaries of varying lithology, and showed unique forms that could often be differentiated from natural fractures. In zones more prone to fracturing (i.e., calcareous rich intervals), both natural and induced fractures were common and preferentially occurred. When both real and artificial fractures were present, they were separated based on their orientation and resistivity. In cases where induced fractures connect and enhance natural fractures, the presence of natural fractures were determined if the fringes of the fracture were more resistive, indicating natural mineralization.

Since the resolution of the FMI log was less than that of core, only a relative fracture density and fracture length was gathered for the FMI log. The number of fractures was determined by adding the total number of distinguishable separate fractures within a one-foot zone. For fracture length, this was done by measuring the vertical length of the fractures in a one foot-length zone and adding the lengths when two or more fractures occur. When both seismic and FMI log fracture orientation interpretations were integrated, these two datasets appeared to be remarkably consistent. Previous authors have described similar patterns. Butler et al (1976) reported that in the Buchan field, smaller scale fractures had the same general orientation as the larger scale faults/fractures. Previous studies conducted ~95 km (60 miles) south of this study area indicated that the left-lateral faulting regime is common in the region (e.g. Moody and Hill, 1956; Tanner, 1967; Thorman, 1969; Wickham, 1978; Butler, 1980; McLean and Stearns, 1983; Harding, 1985; Budnik, 1986; Cox and VanArsdale, 1988). Moreover, the approximately E-W in-situ σ_H orientation estimated in this study appear to be consistent with σ_H orientations estimated by Snee and Zoback (2016). This is significant because these observations may be transferable to basins with similar rocks and similar stress regimes.

Comparing fracture density from core descriptions, FMI log interpretations, and FIV petrophysical evaluations was a reasonable task as the scales progressively increased with some overlap. Due to the fact that the resolution of fractures detectible to the naked eye in core is significantly better than that of the FMI log, and FIV petrophysical interpretations, there were often more detectible fractures in the cores. This resulted in higher fracture densities in the core fracture characterization than that of the FMI log and FIV fracture characterization. Relative fracture density curves appeared to solve the scale, resolution, and depth of investigation challenges associated with these datasets as all showed a relatively consistent fracture density with each dataset validating the other.

The greatest challenge was comparing the vastly different fracture density scales of the seismic interpretations to that of the remaining data sets. The maximum depth of investigation for fracture detection from the FIV analysis comes from the deep resistivity log with a maximum lateral depth of investigation around 2.5 m (~8 feet) and a vertical resolution of a ~0.5 meter (1-2 feet). The calculated maximum vertical and lateral detectable limit of the seismic data in this study were 2.8-3.5 m (9.6-12 feet) and 3.8-3.5 m (12.5-14.70 feet) respectively. Since there was little to no overlap in scales between these datasets, they were related on a gross scale. Although, this showed fair positive correlations, this interpretation could be improved by fracture upscale modelling as shown in Holman (2011). Unfortunately, this method requires FMI logs recorded in the lateral section of a horizontal well to accurately depict lateral fracture variability, which was not available for this study.

Reservoir quality relationships were also investigated, and basic correlations were drawn. The FIV detected fractures demonstrated a positive correlation with increased reservoir quality as indicated by the reservoir quality flags from the FIV analysis. Fractures in this study correlated well with areas of relatively better reservoir quality which indicates that the detected fractures cause an increase in porosity and permeability. This indicated that fractures are not in fact fully mineralized as was interpreted in the core descriptions of this study and in Wang et al. (*2019*). It seems statistically unlikely that the two STACK core studied in this project, and the five STACK core described in Wang et al. (*2019*) did not contain any of the partially open fractures like the FIV analysis showed in this study. Alternatively, it is more likely that at least some of the fractures interpreted in both studies are partially mineralized and contained a pore network that was visibly undetectable in core and image log interpretations. Investigation of the high definition ultra-violate (UV) and white light core images available from Well D, contained fractures which appeared to be fully mineralized to the naked eye but showed light-oil/condensate blue/yellow hydrocarbon fluorescence, further indicating partially open fractures. Additionally, the possibility

of the fractures being partially mineralized instead of fully mineralized supports the suggestion by Wang et al (*2019*), and that has been demonstrated in Babcock (1978), Fisher et al (2002), and Gale et al (2007 and 2014), that fractures may act as planes of weakness that help facilitate the propagation of induced fractures during hydraulic stimulation. This is critical because if these fractures were in fact "fully mineralized" with calcite cement, they could act as energy barriers and pose a hindrance to production by impeding the growth of new hydraulic fractures during hydraulic fracturing treatments as was shown in Gale et al (2014). It is recommended that the presence of partially mineralized fractures is investigated further using scanning electron microscope techniques, thin sections, and porosity and permeability tests to better understand the pore network in the otherwise seemingly fully mineralized fractures.

A strong negative correlation also existed between increasing calcite and decreasing reservoir quality. This is consistent with Shelly (2014), Price et al. (2017), Wang et al (*2019*) Neely (2019). It appeared in the "Meramec" interval, increasing calcite is likely in the form of cement which occludes porosity and permeability (Price et al., 2017; Shelly, 2014). Additionally, within the "Meramec" interval, mineralogy appears to be the dominant variable in determining reservoir quality. This interpretation is in line with the calcareously influenced subaqueous delta complex depositional environment model proposed by Price et al (2017) and described in Patruno et al (2015). Significant calcite cementation is found in silty peloidal turbidites that are believed to have had a higher porosity value upon deposition in areas more proximal to the topset or foreset of the subaqueous clinoform system (Price et al. 2017; Patruno et. Al., 2015). On the other hand, more argillaceous siltstones with lower depositional porosity and higher clay content show smaller amounts of calcite cementation and better preserve inter-particle pore space (Price et al., 2017).

Alternatively, the "Osage" interval, historically defined in this area as a more calcareous rich interval, commonly showed better reservoir quality with the presence of fractures. This has

significant exploration and production implications for both the “Meramec and the Osage” intervals. In the “Meramec” interval, which is dominantly a siliciclastic reservoir, fractured zones should not be the primary target as they are most often associated with an increase in calcite content. In the “Osage” interval on the other hand, it is dominated by calcite mineralogy in most places, and good reservoir quality is often largely dependent on the presence of fractures.

6.2. Conclusions

Integrated data sets are almost always superior in geologic interpretations compared to individual data types as they are more robust in their observations and have a way of quality controlling interpretations at different scales. This study showed that integrating the interpretations of the available seismic, log, and core data from the study area led to the following conclusions:

(1) Fracture orientations and in-situ stress can be assessed within the STACK play in the Anadarko Basin, Oklahoma based on the analysis of stacked seismic data.

(2) Fracture orientations determined from the seismic data can be compared to and constrained by the fracture orientations from the FMI logs.

(3) Large scale seismically detected fractures were found to be oriented in the same direction as the small-scale FMI detected fractures indicating an intrinsic relationship between the two.

(4) Fracture density described in core, FMI logs, fracture petrophysical evaluations, and seismic attributes can be accurately compared and “ground truthed” by each other.

(5) In the STACK, within the “Meramec” interval, an increase in fracture content is likely associated with an increase in calcite content, which typically occludes porosity and overrides the porosity and permeability obtained from the fractures. Fractured zones should not be the primary reservoir target within the “Meramec” interval. Alternatively,

zones with relatively less calcite content, and more clay and silt content typically result in better reservoir quality and should be given preference.

(6) In the STACK, the "Osage" interval, an increase in reservoir quality was found to be associated with an increase in fracture content. Rarely, does the "Osage" achieve better than fair reservoir quality, as defined by the NULOOK FIV analysis, without the addition of fractures. Highly fractured zones within the "Osage" interval were typically associated with an increase in reservoir quality and should be given preference.

(7) In both "Meramec and Osage" intervals, the fractures themselves were shown to improve reservoir quality based on the FIV petrophysical analysis. This indicates that these fractures are not fully mineralized as the original core and FMI log interpretations in this study and Wang et al (*2019*) originally indicated. Subsequent HD UV light core photos indicated light-oil/condensate hydrocarbon fluorescence was present in many of the fractures suggesting the existence of a three-dimensional pore network within the otherwise seemingly fully mineralized fractures. It is recommended that this is studied further with more advanced techniques.

(8) Assuming many of the previously interpreted fractures are in fact partially mineralized, instead of fully mineralized, supports the suggestion by Wang et al (*2019*), that fractures in the STACK may act as planes of weakness that aid the growth of induced fractures during hydraulic fracturing.

(9) The detection of older faults/fractures oriented in different directions, illustrated the remnants of paleo-stress regimes. It showed how the σ_H rotated in orientation from NW during the Silurian time, to NE-ENE during the Mississippian, and finally to E-W during the Pennsylvanian which likely persisted, more or less, to the present day in-situ σ_H orientation. Based on the interpretation of these fractures and other geologic features in

this study area, a simple shear structural deformation model for the STACK play is proposed.

REFERENCES

Adams, J., Bourke, L., and Buck, S., 1990, Integrating formation microscanner images with core: Schlumberger Oilfield Review, v. 2, no. 1, p. 52–65.

Adams, J. T., Garcı´a-Carballido, C., Glass, C., Maddock, R., and Styles, A., 1999, Using borehole images and core to characterize fractures and in-situ stress in hydrocarbon reservoirs, *in* Fracture and in-situ stress characterization of hydrocarbon reservoirs: Geological Society London Conference on Fractures and Stress, unpublished.

Ameen, M.S., *ed*., 2003, Fracture and In-Situ Stress Characterization of Hydrocarbon Reservoirs. Geological Society, London, Special Publications, v. 209, p. 1-6

Aplin, G. F., Sapru, A. K., Lawrence, M. J. F., 2003, Characterization of carbonate reservoir heterogeneity using borehole image logs: Proceedings of the International Geophysical-Geological-Mining of Fluid-Environmental Meeting/Conference and Exhibition, September 19–20, 2003, Szolnok, Hungary, p. 8

Babcock, E. A., 1978, Measurement of subsurface fractures from dipmeter logs: AAPG Bulletin, v. 62, p. 1111–1126.

Badir, M., 2007, Emerging technologies in improving carbonate characterization and hydrocarbon recovery (abs.): Carbonate Reservoir Summit, Bahrain 2007, Abstract Volume, p. 7

Barton, C. A., and Zoback, M. D., 1998, Earth stress, rock fracture and wellbore failure-Wellbore imaging technologies applied to reservoir geomechanics and environmental engineering: 4th Society of Exploration Geophysicists of Japan International Symposium, Tokyo, Japan, December, p. 49–56.

Barton, C. A., Zoback, M. D., Burns, K. L., 1988, In situ stress orientation and magnitude at the Fenton geothermal site, New Mexico, determined from wellbore breakouts: Geophysical Research Letters, v. 15, no. 5, p. 467–470, doi:10.1029/GL015i005p00467.

Barton, C. A., Moos, D., Peska, P., Zoback, M. D., 1997, Utilizing wellbore image data to determine the complete stress tensor: Application to permeability anisotropy and wellbore stability: The Log Analyst, v. 38, no. 6, p. 21–33

Budnik, R. T., 1986, Left-lateral intraplate deformation along the Ancestral Rocky Mountains—Implications for late Paleozoic plate motions: Tectonophysics, v. 132, p. 195 214

Butler, K. R., 1980, A structural analysis of the Cambrian-Ordovician strata on the north flank of the Wichita Mountains, Oklahoma: Geological Society of America Abstracts with Programs, v. 12, no. 1, p. 2.

Butler, M., Phelan, M. J., Wright, A. W. R., 1976, Evaluation of a Fractured Sandstone Reservoir, Transactions, SPWLA Fourth European Symposium, Oct. 18-19, London, England.

Carr, T.R., Merriam, D.F., Bartley, J.D., 2005, Use of relational databases to evaluate regional petroleum accumulation, groundwater flow, and CO2 sequestration in Kansas. AAPG Bulletin; 89 (12): p. 1607–1627.

Childress, M., and Grammer, G. M., 2018, Characteristics of debris flows and outrunner blocks: Evidence for Mississippian deposition on a distally steepened ramp, in G. M. Grammer, J. M. Gregg, J. O. Puckette, P. Jaiswal, M. Pranter, S. J. Mazzullo, and R. H. Goldstein, eds., Mississippian reservoirs of the midcontinent, U.S.A.: AAPG Memoir 116, p. xx–xx.

Chopra, S., and Marfurt, K. J., 2007, Volumetric curvature attributes for fault/fracture characterization: First Break, 25, 19-30.

Cox, R. T., and VanArsdale, R. B., 1988, Structure and chronology of the Washita Valley fault, southern Oklahoma aulacogen: Shale Shaker, v. 39, no. 1, p. 2-13.

Cullen, A. 2017, Devonian-Mississippian Petroleum Systems of Southern Laurasia: What Makes the “STACK”-Merge-SCOOP Play in Oklahoma so Special: AAPG, Search & Discovery Article #10998.

Dorn, G., 2018, Resolution & Detection is Seismic Data and the Detectable Limits of the relative amplitude change method in Seismic Data, CGG-Geosoftware, Technical Report, p. 1

CGG-GeoSoftware, 2018, InsightEarth® Technical Reference, Version 3.4.0, p. 1-415

CGG-GeoSoftware, 2015, Structural interpretation of Geology with InsightEarth®. Course # TS-200, Student Guide, Version 3.0, p. 1-177

Denison, R.E., 1982, Geologic cross section from the Arbuckle Mountains to the Muenster Arch in southern Oklahoma and Texas: Geological Society of America Map and Chart Series MC-28R, 8 p.

Fisher, M. K., Wright, C. A., Davidson, B. M., Goodwin, A. K., Fielder, E. O., Buckler, W. S., Steinsberger, N. P., 2002, Integrating fracture mapping technologies to optimize stimulations in the Barnett Shale: SPE Annual Technical Conference and Exhibition Article #77441, San Antonio, Texas, September 29–October 2, 2002.

Fossen, H., 2010, Structural Geology, University of Cambridge Press, ch. 5, p. 80

Gale, J. F., Reed, R. M. and Holder, J., 2007, Natural fractures in the Barnett Shale and their importance for hydraulic fracture treatments: AAPG Bulletin, v. 91, p. 603–622.

Gale, J. F.W., Laubach, S. E., Olson, J. E., Eichhubl, P., Fall, A., 2014, Natural fractures in shale: A review and new observations: AAPG Bulletin, v. 98, p. 2165–2216.

Ham, W.E., Denison, R.E., Merritt, C.A., 1964, Basement rocks and structural evolution of southern Oklahoma: Oklahoma Geological Survey Bulletin 95, p. 302

Hansen, B., and Buczak, J., 2010, Making interpretable images from image logs, *in* M. Po¨ppelreiter, C. Garcı´aCarballido, and M. Kraaijveld, ed., Dipmeter and borehole image log technology: AAPG Memoir 92, p. 51–66.

Harding, T. P., 1985, Seismic characteristics and identification of negative flower structures, positive flower structures, and positive structural inversion: American Association of Petroleum Geologists Bulletin, v. 69, no. 4, p. 582-600.

Hesthammer, J., and Fossen, H., 2003, From seismic data to core data: An integrated approach to enhance reservoir characterization, *in* M. Ameen, ed., Fractures and in-situ stress characterization of hydrocarbon reservoirs: Geological Society (London) Special Publication 209, p. 39–54.

Hesthammer, J., Landro, M., Fossen, H., 2001, Use and abuse of seismic data in reservoir characterization: Marine and Petroleum Geology, v. 18, p. 634-655

Higley, D. et al., 2014, Assessment of Undiscovered Oil and Gas Resources of the Anadarko Basin Province of Oklahoma, Kansas, Texas, and Colorado 2010, US Geological Survey Digital Data Series DDs-69-EE, Chapters 1-13.

Hill, B., 2009, Finding Naturally Fractured Producing Intervals Using Conventional Well Logs, Nutech Energy Alliance, Technical Report, p.1-2

Holman, R., 2011, Seismic Characterization of Fractured Rock Fabric in Mississippian Limestone, Payne County Oklahoma. Master's thesis, Oklahoma State University, Stillwater, Oklahoma, p. 1-131

Hurley, N., 2004, Borehole Images, *in* Asquith, G., Krygowski, D., ed., Basic Well Log Analysis: AAPG Methods in Exploration 16, ch. 9, p. 151-163

Kulander, B.R., Dean, S.L., Ward, B.J., 1990, Fractured Core Analysis: Interpretation, Logging, and Use of Natural and Induced Fractures in Core: AAPG, Methods in Exploration Series, v. 8, p. 1-8

Leckie, R.M., Sigurdsson, H., Acton, G.D., and Draper, G. ed., 2000 Proceedings of the Ocean Drilling Program, Scientific Results, v. 165, p. 205-217

Lei, Q., Latham, J.P., Tsang, C.F., 2017, The use of discrete fracture networks for modelling coupled geomechanical and hydrological behaviour of fractured rocks, Computers and Geotechnics Journal, v. 85, p. 151-176

Liu, E., Johns, M., Zelewski, G., Burnett, W. A., Wu, X., Zhang, J., … Al Messabi, A., 2015, Fracture Characterization by Integrating Seismic-Derived Attributes including Anisotropy and Diffraction Imaging with Borehole Fracture Data in an Offshore Carbonate Field, United Arab Emirates. International Petroleum Technology Conference. IPTC-18533-MS, p. 1-21

Marfurt, K. J., Kirlin, R. L., Farmer, S. L., Bahorich, M. S., 1998, 3-D seismic attributes using a semblance-based coherency algorithm: Geophysics, 63, 1150–1165.

McLean, R. and Stearns, D.W., 1983, Fault analysis in Wichita Mountains [abs.]: American Association of Petroleum Geologists Bulletin, v. 76, no. 3, p. 511-512.

Moody, J. D., and Hill, M. J., 1956, Wrench-fault tectonics: Geological Society of America Bulletin, v. 67, no. 9, p. 1207-1246.

Neely, W., 2019, Seismic Characterization of the Reservoir Heterogeneity within the "Meramec" Interval Of The "Stack" Play in the Anadarko Basin of Central Oklahoma, Master's thesis, Oklahoma State University, Stillwater Oklahoma

Nutech Energy Alliance, 2018, Pay Flags and NULIST Descriptions, Technical Reference, p. 1

Perry, W.J., 1989, Tectonic Evolution of the Anadarko Basin Region, Oklahoma, United States Geological Survey Bulletin 1866, ch. A, p. 1-19

Pranter, M.J., Hurley, N.F., Davis, T.L., 2004, Sequence-Stratigraphic, Petrophysical, and Multicomponent Seismic Analysis of a Shelf-Margin Reservoir: San Andres Formation (Permian), Vacuum Field, New Mexico, United States, *in* Eberli, G.P., Masaferro, L.J., Sarg, J.F., ed., Seismic Imaging of Carbonate Reservoirs and Systems, AAPG Mem. 81, ch. 3, p. 59-89

Price, B. J., and Grammer, G. M., 2018, High resolution sequence stratigraphic architecture and reservoir characterization of the Mississippian Burlington–Keokuk Formation, northwestern Arkansas, U.S.A., in G. M. Grammer, J. M. Gregg, J. O. Puckette, P. Jaiswal, M. Pranter, S. J. Mazzullo, and R. H. Goldstein, eds., Mississippian reservoirs of the midcontinent, U.S.A.: AAPG Memoir 116, p. xx–xx.

Price, B., Haustveit, K., Lamb, A., 2017, Influence of Stratigraphy on Barriers to Fracture Growth and Completion Optimization in the Meramec Stack Play, Anadarko Basin, Oklahoma: Unconventional Resources Technology Conference, 2697985.

Redger, C., 2015, Seismic Attribute Analysis of the upper Morrow Sandstone and the Arbuckle Group from 3D-3C Seismic Data at Cutter Field, Southwest Kansas, Master's thesis, University of Kansas, Lawrence, Kansas, p. 119

Shafiei, A., Dusseault, M.B., Kosari, E., Taleghani, M.N., 2018, Natural Fractures Characterization and In Situ Stresses Inference in a Carbonate Reservoir—An Integrated Approach, Energies Journal, v. 11, 312, p. 1-26

Shalaby, M.R., and Islam, M.A., 2017, Fracture detection using conventional well logging in carbonate Matulla Formation, Geisum oil field, southern Gulf of Suez, Egypt. Journal of Petroleum Exploration and Production Technology, v. 7, p. 977-989

Shelly, S., 2014, Outcrop-Based Sequence Stratigraphy and Reservoir Characterization of an Upper Mississippian Mixed Carbonate Siliciclastic Ramp, Mayes County, Oklahoma, Master's thesis, Oklahoma State University, Stillwater, Oklahoma, p. 92

Snee, L.J.E., and Zoback, M.D., 2016, State of stress in Texas: Implications for induced seismicity. American Geophysical Union, Research Letter, v. 43, p. 1-7

Stukey, B., Godwin, C., Puckette, J., 2018, Biostratigraphically Constrained Ages of Mississippian Mixed Carbonate-Siliciclastic Sequences, STACK Play, Andadarko Basin, Oklahoma. Oklahoma Geological Survey, The STACK Play Workshop, Technical Presenation #4

Suau, J., Gartner, J., 1980, Fracture Detection from Well Logs. The Log Analyst, p. 3-13

Tanner, J. H., 1967, Wrench fault movements along Washita Valley fault, Arbuckle Mountain area, Oklahoma: American Association of Petroleum Geologists Bulletin, v. 51, p. 126-141.

Thorman, C. H., 1969, Wrench faulting in southern Oklahoma [abs.]: Geological Society of America Special Paper 121, p. 571.

Tinker, S.W., Caldwell, D.H., Cox, D.M., Zahm, L.C., Brinton, L., 2004, Integrated Reservoir Characterization of a Carbonate Ramp Reservoir, South Dagger Draw Field, New Mexico: Seismic Data Are Only Part of the Story, *in* Eberli, G.P., Masaferro, L.J., Sarg, J.F., ed., Seismic Imaging of Carbonate Reservoirs and Systems, AAPG Mem. 81, ch. 4, p. 91-105

Walker, J.D., Geissman, J.W., Bowring, S.A., and Babcock, L.E., compilers, 2018, Geologic Time Scale v. 5.0: Geological Society of America, https://doi.org/10.1130/2018.CTS005R3C. ©2018 The Geological Society of America

Wang, Y., T. Thompson, and G. M. Grammer, 2019 (in press), Fracture characterization and prediction in unconventional reservoirs of the "Mississippian limestone," north-central Oklahoma, United States, in G. M. Grammer, J. M. Gregg, J. O. Puckette, P. Jaiswal, S. J.

Mazzullo, M. J. Pranter, and R. H. Goldstein, eds., Mississippian reservoirs of the midcontinent: AAPG Memoir 122, doi:10.1306/13632151M1163789

Wickham, J.S., 1978, The southern Oklahoma aulacogen, in Structural style of the Arbuckle region: Geological Society of America South-central Section, Field Trip Guidebook 3, p. 8-41.

Wittman, B.R., 2013, Subsurface Stratigraphy and Characterization of Mississippian (Osagean to Meramecian) Carbonate Reservoirs of the Northern Anadarko Shelf, North-Central Oklahoma, *Theses and Dissertations*, 728

VITA

Joshua Michael Andrew Bedell

Candidate for the Degree of

Master of Science

Thesis: INTEGRATED FRACTURE AND STRESS CHARACTERIZATION, MISSISSIPPIAN "MERAMEC AND OSAGE" INTERVALS, STACK PLAY, CENTRAL OKLAHOMA

Major Field: Geology

Biographical:

Education:

Completed the requirements for the Master of Science in Geology at Oklahoma State University, Stillwater, Oklahoma in May, 2019.

Completed the requirements for the Bachelor of Science in Geology at Oklahoma State University, Stillwater, Oklahoma, USA in 2017.

Experience:
Present | Geophysicist | Exploration New Ventures | Devon Energy, OKC, OK
2018 | Geoscience Intern | L48 New Ventures | ConocoPhillips, Houston, TX
2017 | Geoscience Intern | Permian Basin BU | ConocoPhillips, Houston, TX
2013-17 Petroleum Landman | Sooner Mineral Investments, OKC, OK

Professional Memberships:
American Association of Petroleum Geologists, Society of Exploration Geophysicists, Society of Petroleum Engineers, Oklahoma City Geological Society